General Disclaimer

One or more of the Following Statements may affect this Document

- This document has been reproduced from the best copy furnished by the organizational source. It is being released in the interest of making available as much information as possible.

- This document may contain data, which exceeds the sheet parameters. It was furnished in this condition by the organizational source and is the best copy available.

- This document may contain tone-on-tone or color graphs, charts and/or pictures, which have been reproduced in black and white.

- This document is paginated as submitted by the original source.

- Portions of this document are not fully legible due to the historical nature of some of the material. However, it is the best reproduction available from the original submission.

DRA

FINAL REPORT NASA GRANT NAG-1-316

August 15, 1983

AN INVESTIGATION OF THE ACCURACY OF FINITE DIFFERENCE METHODS

IN THE SOLUTION OF LINEAR ELASTICITY PROBLEMS

Principal Investigators

Nelson R. Bauld, Jr.
James G. Goree

Department of Mechanical Engineering
College of Engineering
Clemson University
Clemson, South Carolina 29631

FINAL REPORT NASA GRANT NAG -1-316

August 15, 1983

AN INVESTIGATION OF THE ACCURACY OF FINITE DIFFERENCE METHODS

IN THE SOLUTION OF LINEAR ELASTICITY PROBLEMS

Principal Investigators

Nelson R. Bauld, Jr.
James G. Goree

Professors of Mechanics and
Mechanical Engineering
Clemson University
Clemson, South Carolina   29631

Graduate Assistant

Lih-Shyng Tzeng

Ph.D. Candidate in
Engineering Mechanics

ABSTRACT

This study considers the accuracy of the finite difference method in the solution of linear elasticity problems that involve either a stress discontinuity or a stress singularity. Solutions to three elasticity problems are discussed in detail: a semi-infinite plane subjected to a uniform load over a portion of its boundary; a bimetallic plate under uniform tensile stress; and a long, midplane symmetric, fiber-reinforced laminate subjected to uniform axial strain.

Finite difference solutions to the three problems are compared with finite element solutions to corresponding problems. For the first problem a comparison with the exact solution is also made.

The finite difference formulations for the three problems are based on second order finite difference formulas that provide for variable spacings in two perpendicular directions. Forward and backward difference formulas are used near boundaries where their use eliminates the need for fictitious grid points. Moreover, forward and backward finite difference formulas are used to enforce continuity of interlaminar stress components for the third problem.

The study shows that the finite difference method employed in this investigation provides solutions to the three elasticity problems considered that are as accurate as the corresponding finite element solutions. Furthermore, the finite difference method appears to give a solution for the laminate problem that characterizes the stress distributions near an interface corner in a more realistic manner than the finite element method.

ACKNOWLEDGEMENTS

TABLE OF CONTENTS

LIST OF TABLES

LIST OF FIGURES

List of Figures (cont.)

I. INTRODUCTION

A serious failure mechanism for laminated composite materials is edge delamination. Various numerical methods have been used in attempts to calculate the interlaminar stress components that accompany delamination in a finite-width $[\pm 45]_s$ angle-ply laminate under uniform axial strain [1,2,3,4]. These efforts have resulted in serious discrepancies in reported behavior for the interlaminar normal stress distribution near an interface corner [4]. For example, a finite-difference procedure [1] and a perturbation procedure [2] predict tensile interlaminar normal stress near an interface corner, while finite element methods [3,4] predict compressive normal stress in this region. Furthermore, some uncertainty exists regarding the character of the in-plane, interlaminar normal and shearing stress distributions near an interface corner that are predicted by finite element methods [3,4].

The primary purpose of this investigation is to determine if the finite difference method is capable of providing accurate predictions for the interlaminar stress components near an interface corner and, hence nea a stress singularity.

A second purpose of this investigation is to determine if predictions, by finite element methods, for in-plane, interlaminar stress components near an interface corner accurately represent laminate behavior; and, if these predictions are spurious, to cast light on the origin of the weakness in the finite element method that results in the spurious behavior.

In this investigation the finite difference method has been used to obtain numerical solutions for three different problems that involve a point where a stress component becomes discontinuous or singular. These

problems are: (a) uniform pressure on part of a semi-infinite plane (Figure 1a), (b) a bimetallic plate under uniform axial tension (Figure 5a), and (c) a finite-width $[\pm 45]_s$ angle-ply laminate under uniform axial strain (Figure 8a). Solutions to each of these problems via finite element methods are reported in reference [4].

The finite difference procedure used in this investigation provides for variable grid spacings in two perpendicular directions. Consequently, computational efficiency is effected by taking closely spaced grid lines in regions where the stress components are expected to vary rapidly, and a coarser grid in regions where the stress components do not vary rapidly.

The coefficient matrix corresponding to the system equations is unsymmetrical; therefore, it is necessary to store the entire band of the coefficient matrix. Moreover, an equation solver capable of handling un- symmetrical systems of algebraic equations must be available. Nevertheless, variable grid capability leads to more efficient computations than finite difference procedures that use uniform spacing because substantially fewer grid lines are needed to realize an accuracy comparable to the accuracy associated with a specific uniform grid.

II. DISTRIBUTED LOAD ON A SEMI-INFINITE PLANE

Figure 1a depicts a semi-infinite plane that is subjected to a uniform pressure on part of the edge y=0. The exact solution for this problem is given in reference [4] and indicates that $\sigma_{xy}(\pm a, 0) = \mp p/\pi$ when the points $(\pm a, 0)$ are approached along the lines $x = \pm a$. Consequently, $\sigma_{xy} \neq \sigma_{yx}$ at these points.

It is of interest in this investigation to obtain a numerical solution for this problem based on the finite difference method, and to compare the finite difference, finite element, and exact solutions for the stress distributions $(\sigma_x, \sigma_y, \sigma_{xy})$ along the lines $x = \pm a$.

For discretization purposes it is assumed that the stress component are nearly zero for $x \geq \pm$ 10a, and that vertical displacements are essentially zero at a depth $y \geq$ 10a. Moreover, for computational efficiency use is made of symmetry with respect to the line $x = 0$.

Boundary Value Problem. The field equations associated with the distributed load problem are listed below.

Stress-Strain Relations

$$\left.\begin{aligned}
\sigma_x &= \frac{E}{1-\nu^2} (\varepsilon_x + \nu\varepsilon_y) \\
\sigma_y &= \frac{E}{1-\nu^2} (\varepsilon_y + \nu\varepsilon_x) \\
\sigma_{xy} &= \sigma_{yx} = \frac{E}{2(1+\nu)} \varepsilon_{xy}
\end{aligned}\right\} \tag{1}$$

Strain-Displacement Relations:

$$\left.\begin{aligned}
\varepsilon_x &= u_{,x} \\
\varepsilon_y &= v_{,y} \\
\varepsilon_{xy} &= \varepsilon_{yx} = u_{,y} + v_{,x}
\end{aligned}\right\} \tag{2}$$

Equilibrium Equations (Plane Stress):

$$\left.\begin{aligned}
(u_{,xx} + \nu v_{,xy}) + \frac{1}{2}(1-\nu)(u_{,yy} + v_{,xy}) &= 0 \\
(v_{,yy} + \nu u_{,xy}) + \frac{1}{2}(1-\nu)(v_{,xx} + \nu u_{,xy}) &= 0
\end{aligned}\right\} \tag{3}$$

Boundary Conditions:

$$\left.\begin{aligned}
u(0,y) &= v_{,x}(0,y) = 0 \\
\sigma_x(10a,y) &= \sigma_{xy}(10a,y) = 0
\end{aligned}\right\} \quad 0 \leq y \leq 10a$$

$$\left.\begin{aligned}
\sigma_{yx}(x,0) = 0, \quad 0 \leq x \leq 10a; \quad \sigma_y(x,0) &= \begin{cases} -p & 0 \leq x < a \\ -p/2 & x = a \\ 0 & a < x \leq 10a \end{cases} \\
\sigma_{yx}(x,10a) = v(x,10a) = 0 \qquad 0 \leq x \leq 10a
\end{aligned}\right\} \tag{4}$$

-3-

<u>Numerical Results</u>. The finite-difference grid used to analyze this problem
is shown in Figure 1b. Vertical grid lines are more closely spaced on either
side of the line x = a, while the horizontal grid lines are more closely
spaced near the line y = 0. Numerical values of grid spacings for the
x and y directions are listed in Table I. The numerical results to be
discussed are based on these spacings which correspond to 2,146 degrees of
freedom.

In Figures 2 and 3 the open circles and dashed lines represent numerical
solutions obtained via the finite difference and finite element methods,
respectively, and the solid lines represent the exact solution, for the
stress components σ_x, σ_y and σ_{xy} along the line x = a. The finite dif-
ference and finite element solutions for $\sigma_x(a,y)$ and $\sigma_y(a,y)$ exhibit excellent
agreement everywhere. The finite difference and finite element solutions
for $\sigma_{xy}(a,y)$ show excellent agreement with the exact solution except near
the point (a,0) where the finite difference solution appears to provide a
somewhat better agreement - except for the first two nodes of the finite
difference grid. The finite difference solution for $\sigma_{xy}(a,y)$ is "drawn"
to zero by the enforced zero shearing stress at the boundary, while the
finite element solution is "drawn" down but not to a zero value at the
boundary.

It appears that requiring the stress tensor to be symmetrical at the
point (a,0) affects the finite difference solution for the shearing stress
$\sigma_{xy}(a,y)$ only in a small region that is confined to the first two finite
difference grid points. This region can be made as small as desired, con-
tingent on numerical limitations.

The finite difference solution for the stresses σ_x, σ_y, and σ_{xy} shown in Figure 2 is based on a boundary value $\sigma_y = - p/2$ at the point $(a,0)$; that is, on an average of the boundary load intensity to the left and right of the point $(a,0)$. A finite difference solution using $\sigma_y(a,0) = - p$ differs from this solution only in a small region near the point $(a,0)$ as shown by the open circles and solid curves in Figures 4a, 4b, and 4c. From these figures it is seen that $\sigma_{xy}(a,y)$ is essentially the same for either $\sigma_y(a,0) = - p/2$ or $\sigma_y(a,0) = - p$, while the solutions for σ_y and σ_x are affected dramatically in the vicinity of $y = 0$. Otherwise, the finite difference solutions using $\sigma_y(a,0) = - p/2$ or $\sigma_y(a,0) = - p$ are essentially identical.

Since the stress tensor is unsymmetrical at the point $(a,0)$ it was of interest to determine if a more accurate representation of the behavior of $\sigma_{xy}(a,y)$ could be obtained near the point $(a,0)$ by discarding the symmetry relation $\sigma_{xy} = \sigma_{yx}$ at this point and replacing it with a finite moment equation that would require $\sigma_{yx}(a,0) = 0$, but $\sigma_{yx}(a,0) \neq \sigma_{xy}(a,0)$. In addition to the finite moment equation, a finite force equilibrium was introduced. The stress distributions for σ_y and σ_x are essentially identical to the finite-difference solution for $\sigma_y(a,0) = - p/2$ and $\sigma_{yx}(a,0) = \sigma_{xy}(a,0) = 0$ everywhere (solid lines in Figures 4b and 4c). The shearing stress distribution differs only in the neighborhood of the point $(a,0)$. The shearing stress $\sigma_{xy}(a,y)$ for the case $\sigma_{yx}(a,0) \neq \sigma_{xy}(a,0)$ is indicated by the dashed line in Figure 4a.

III. BIMETALLIC PLATE UNDER UNIFORM TENSION

Figure 5a depicts a bimetallic plate under uniform tensile stress along the edges y = ± 8a with stress-free boundaries at the edges x = 0, 8a. A numerical solution for the stress components along the bond line, based on the finite element method, is given in reference [4] for a rigid bottom plate.

It is of interest in this investigation to obtain a numerical solution for the stress components along the bond line using the finite-difference method, and to compare this solution with the finite element solution obtained in reference [4]. It is of particular interest to observe whether the finite difference method is capable of predicting the behavior of the shearing stress component near the intersections of the bond line and the free edges.

Boundary Value Problem. The plane strain field equations for the bimetallic plate with a rigid bottom plate are obtained from the plane stress field equations given by Equations (1)-(3) by replacing E and ν in these equations by $E^* = E/(1-\nu^2)$ and $\nu^* = \nu/(1-\nu)$ and affixing the boundary conditions

$$
\left.
\begin{array}{l}
\left.
\begin{array}{l}
\sigma_x(0,y) = \sigma_{xy}(0,y) = 0 \\
\\
u(4a,y) = v_{,x}(4a,y) = 0
\end{array}
\right\} \quad 0 \le y \le 8a \\
\\
\\
\left.
\begin{array}{l}
u(x,0) = v(x,0) = 0 \\
\\
\sigma_{yx}(x,8a) = 0, \quad \sigma_y(x,8a) = p
\end{array}
\right\} \quad 0 \le x \le 4a
\end{array}
\right\} \quad (5)
$$

These boundary conditions make use of symmetry with respect to the plate centerline x = 4a.

<u>Numerical Results</u>. Figure 5b shows the finite-difference grid used to analyze the bimetallic plate problem. Since the bond line stress components are expected to change rapidly near the singular point 0, the finite difference grid lines are more closely spaced in the region near point 0. Numerical values of spacings for the x and y directions are listed in Table II. Numerical results presented in this section are based on these grid spacings which correspond to 2,340 degrees of freedom.

Corner points of a rectangular finite difference grid are usually troublesome because a decision must be made as to which of two possible sets of boundary conditions to employ there. In the present investigation it was physically appealing to require the displacement components (u,v) at the corners of the bond line to be specified (as zero), since the two plates do not separate there. Moreover, at the left corner of the loaded edge (0,8a) boundary conditions associated with the stress free edge were imposed, while at the right corner of the loaded edge (4a,8a) the conditions $\sigma_y = p$ and u=0 were imposed. Boundary conditions and grid points to which they apply are shown in Figure 5b.

The open circles and dashed curves in Figure 6a represent the finite difference and finite element predictions for the shearing stress distribution along the bond line, respectively. This figure indicates that the finite difference method has no more trouble predicting the stress distribution along the bond line than the finite element method. Indeed the two numerical solutions are essentially the same.

Figure 6b shows the shearing stress and normal stress distributions along the free edge $x = 0$ based on the finite difference method. Both σ_{xy} and σ_x are zero at every finite difference grid point at which these stresses were required to be zero. They were nonzero only at the corner point of the bond line. It is noted that values of σ_{xy} and σ_x at this corner point are calculated from the stress-strain relations and represent limiting values of internal stresses as the corner point is approached along the bond line. They are not necessarily the boundary values on the edge $x = 0$ at $y = 0$. This observation again suggests that the stress tensor is unsymmetrical at a stress singularity.

Figure 7 shows a comparison of the bond line shearing stress distribution for two different finite difference grids. The solid curve with open circles represents the finite difference prediction based on the grid spacings shown in Table II. This curve is an exploded view of the behavior or the shearing stress $\sigma_{xy}(x,0)$ near the point 0 that is exhibited in Figure 6a. The dashed curve with open squares represents the finite difference prediction based on the grid spacings shown in Table III. This finite difference grid maintains the same number of rows and columns as the grid of Table II, but the grid lines parallel to both the x and y directions are redistributed so that they are more dense near point 0.

IV. FOUR-PLY LAMINATE UNDER UNIFORM AXIAL STRAIN

Figure 8a depicts a long, midplane symmetric laminate of width 2b. The laminate consists of four plies, each of thickness h, and is loaded by a uniform axial strain ε_o . Various numerical methods have been used by different investigators [1,2,3,4,] to predict the distributions of normal and shearing stresses between adjacent lamina. Of particular importance is the reliability of a particular numerical method to provide a reasonably accurate assessment of the behavior of the interlaminar stress components near the intersection of an interface with a free edge. This point of intersection is referred to as the interface corner [4] and is shown in Figure 8a.

Computations based on the finite element method have yielded stress distributions that appear to be reasonable for all interlaminar stress components except very near the interface corner. At the interface corner the predicted distributions for the inplane, interlaminar stress components $(\sigma_x, \sigma_y,$ and $\sigma_{xy})$ tend to digress from a logical extrapolation of the stress distributions predicted for interior points along the interface. It is of interest in this investigation to determine whether this digressive behavior exhibited by the finite element method represents actual laminate behavior or, if the predictions are spurious, to illuminate the origin of the weakness in the finite element method that results in this spurious behavior.

A second objective of this investigation is to assess the viability of the finite difference method as an effective numerical method in the computation of interlaminar stress distributions, particularly near an interface corner.

It is customary when dealing with this problem to make use of geometric and material symmetries, thereby making it necessary to consider only the part of the laminate that lies in the first quadrant of the yz plane. This part of the laminate is emphasized by the cross-hatched area in Figure 8a. The heavy dot in this figure is at the interface corner.

Boundary Value Problem. The field equations [1] associated with the four-ply, $[\pm 45]_s$ laminate are listed below.

Stress-Strain Relations:

$$
\left.
\begin{aligned}
\sigma_x &= C_{11}\varepsilon_0 + C_{12}\, V_{,y} + C_{13}\, W_{,z} \pm C_{16}\, U_{,y} \\[4pt]
\sigma_y &= C_{12}\varepsilon_0 + C_{11}\, V_{,y} + C_{13}\, W_{,z} \pm C_{16}\, U_{,y} \\[4pt]
\sigma_z &= C_{13}(\varepsilon_0 + V_{,y}) + C_{33}\, W_{,z} \pm C_{36}\, U_{,y} \\[4pt]
\sigma_{zy} &= C_{44}(W_{,y} + V_{,z}) \\[4pt]
\sigma_{zx} &= C_{44}\, U_{,z} \\[4pt]
\sigma_{xy} &= \pm C_{16}(\varepsilon_0 + V_{,y}) \pm C_{36}\, W_{,z} + C_{66}\, U_{,y}
\end{aligned}
\right\}
\tag{6}
$$

Equilibrium Equations:

$$
\left.
\begin{aligned}
C_{66}\, U_{,yy} + C_{55}\, U_{,zz} \pm C_{26}\, V_{,yy} \pm C_{36}\, W_{,yz} &= 0 \\[4pt]
\pm C_{26}\, U_{,yy} + C_{22}\, V_{,yy} + C_{44}\, V_{,zz} + (C_{23} + C_{44})W_{,yz} &= 0 \\[4pt]
\pm C_{36}\, U_{,yz} + (C_{23} + C_{44})V_{,yz} + C_{44}\, W_{,yy} + C_{33}\, W_{,zz} &= 0
\end{aligned}
\right\}
\tag{7}
$$

Displacement distribution:

$$
\left.
\begin{aligned}
u(x,y,z) &= \varepsilon_0\, x + U(y,z) \\[4pt]
v(x,y,z) &= V(y,z) \\[4pt]
w(x,y,z) &= W(y,z)
\end{aligned}
\right\}
\tag{8}
$$

Boundary Conditions:

$$U(0,z) = V(0,z) = W_{,y}(0,z) = 0 \qquad 0 < z \le 2h \qquad \text{(9a)}$$

$$U(0,0) = V(0,0) = W(0,0) = 0 \qquad z = 0 \qquad \text{(9b)}$$

$$\sigma_{y\ell}(b,z) = \sigma_{yx\ell}(b,z) = \sigma_{yz\ell}(b,z) = 0 \qquad 0 \le z < h \qquad \text{(9c)}$$

$$\sigma_{yu}(b,z) = \sigma_{yxu}(b,z) = \sigma_{yzu}(b,z) = 0 \qquad h < z \le 2h \qquad \text{(9d)}$$

$$U_{,z}(y,0) = V_{,z}(y,0) = W(y,0) = 0 \qquad \text{(9e)}$$

$$\sigma_{zu}(y,2h) = \sigma_{zxu}(y,2h) = \sigma_{zyu}(y,2h) = 0 \qquad 0 \le y \le b \qquad \text{(9f)}$$

$$\sigma_{zu}(y,h) = \sigma_{z\ell}(y,h)$$

$$\sigma_{zxu}(y,h) = \sigma_{zx\ell}(y,h) \qquad 0 \le y \le b \qquad \text{(9g)}$$

$$\sigma_{zyu}(y,h) = \sigma_{zy\ell}(y,h)$$

In Equations (6) and (7) the upper sign (plus sign) is associated with the upper ply (+ 45 ply) and the lower sign (minus sign) is associated with the lower ply (- 45 ply). Equations (8) are fundamental assumptions regarding the distribution of the displacement components u,v and w and are given in reference [1].

Equations (9a) are the conditions associated with laminate symmetry with respect to the z axis, and Equations (9b) are required to exclude rigid body motions. Equations (9c) and (9d) require that the edge at y = b be stress-free, except at the interface corner. Equations (9e) result from symmetry conditions with respect to the y axis, and Equations (9f) require that the edge at z = 2h be stress-free. Finally, Equations (9g) require that the interlaminar stress components be continuous across the interface.

It is particularly important to observe that along the stress-free boundary
(y = b) the formulas that express the stress components σ_y and σ_{yx} in terms
of displacements (Equations 6) are different for the upper and lower plies.
Consequently, the boundary conditions that should be applied at the point (b,h)
are not immediately obvious. This observation is a possible clue as regards the
behavior of the finite element method near the interface corner.

Numerical Results. The following strategy was used to formulate a finite dif-
ference model of the four-ply laminate.

Initially each ply is considered to occupy a separate, independent region.
Separate, independent finite difference grids are assigned to the regions
occupied by the two plies. Subsequently, the finite difference module cor-
responding to the equilibrium equations that are associated with a particular
ply is applied to each grid point that does not lie on the boundary of the
region occupied by that ply. The two regions are connected appropriately by
requiring the displacements (U,V,W) and the interlaminar stress components
(σ_z, σ_{zy}, and σ_{zx}) be continuous across the boundary common to the two plies.

This approach leads logically to the required boundary condition at the
interface corner. That is, the interlaminar stress components should be
required to be continuous across the interface at the interface corner. Thus,
the need to formulate a boundary condition at the interface corner that
accounts for the boundary stresses associated with the +45 and -45 plies in
an equitable manner is avoided.

It will be observed later that the preceding strategy results in predic-
tions for stress distributions that agree well with the finite element predic-
tions away from the interface corner, and also behave in a much more logical
manner near the interface corner. Furthermore, the affect that prescribing
boundary stresses at the interface corner, (instead of interlaminar stress

continuity) has on the stress distributions will be demonstrated. These observations provide a clue as to the puzzling behavior of the finite element method near the interface corner.

The finite difference grid used to analyze this problem is shown in Figure 9. Since the displacement components (U,V,W) are required to be continuous across the interface, the grids associated with the two plys are shown connected in Figure 9. Vertical grid lines are more closely spaced near the interface corner where the stress components are expected to change rapidly, and the horizontal grid lines are more closed spaced about the interface. Numerical values of grid spacings for the y and z directions are listed in Table IV. The numerical results to be discussed are based on these spacings which correspond to 1989 degrees of freedom.

Boundary conditions and the grid points to which they are applied, for what is referred to here as the principal finite difference solution, are shown in Figure 9.

Finite difference solutions for three other sets of boundary conditions at the interface corner are also discussed. These solutions require either $\sigma_{yu} = \sigma_{yxu} = \sigma_{yzu} = 0$ or $\sigma_{y\ell} = \sigma_{yx\ell} = \sigma_{yz\ell} = 0$ or $(\sigma_y)_{ave} = (\sigma_{yx})_{ave} = (\sigma_{yz})_{ave} = 0$ at the interface corner. All other boundary conditions remain the same for each of the four cases. Here $(\sigma)_{ave} = (\sigma_u + \sigma_\ell)/2$ at the interface corner.

Because the interlaminar stress continuity requirements at the interface corner must be relaxed when any of the described sets of conditions are employed, discontinuities in the interlaminar stress components (σ_z, σ_{zx}, and σ_{zy}) are expected at the interface corner.

Case I: Principal Finite Difference Solution. As was stated previously the boundary conditions and the grid points to which they are applied are depicted in Figure 9. Especially important is that continuity of the interlaminar stress

components (σ_z, σ_{zx}, and σ_{zy}) is required along the interface, including the interface corner.

Figures 10 and 11 compare the finite element and the finite difference predictions for stress distributions along the interface between the $+45$ and -45 plies. The open circles connected by a solid curve represent the finite difference predictions and the open squares connected by dashed curves represent the finite element solution.

It is convenient in discussing the behavior of the stresses along the interface to segregate them into two groups: the in-plane components σ_x, σ_y, and σ_{xy}, and the interlaminar components σ_z, σ_{zx}, and σ_{zy}. The first group of stresses must be identified with a particular ply, even at the interface, because they are calculated from stress-strain relations that are different for each ply. The second group of stresses act between the plies and are truly interlaminar stresses. They are equal in magnitude owing to the interlaminar stress continuity requirements.

Consider first the interlaminar stress components. Figure 10 indicates that the finite difference and finite element predictions for the normal stress σ_z are in excellent agreement. Most importantly both predict a large compressive stress at the interface corner and a small tensile region just interior to the interface corner. The lower most curve in Figure 11 depicts the finite difference distribution for σ_{zx} along the interface. The finite element prediction essentially coincides with the finite difference prediction except at the interface corner and is not shown in the figure. The two numerical methods do, however, predict similar behavior at the interface corner; that is, the existence of a stress singularity for the component σ_{zx}.

The finite difference method predicts $\sigma_{zy} \equiv 0$ along the interface, including the interface corner. This agrees with the finite element prediction

except near the interface corner where the finite element method predicts a sudden increase in σ_{zy}.

Now consider the distributions of the in-plane stress components (σ_x, σ_y, σ_{xy}) along the interface. Figure 11 compares these distributions with corresponding distributions predicted by the finite element method.

Figure 11 shows that the finite element and finite difference predictions for each of the in-plane stress components are in excellent agreement except near the interface corner. The finite difference method suggests that the in-plane stress components become singular at the interface corner, while the finite element method predicts a sudden attenuation in the stress components at the interface corner.

Figure 12 shows a comparison of the finite difference and finite element predictions for the distribution of σ_z along the free edge. Excellent agreement is again observed.

Figures 13, 14 and 15 show the variation in free edge stress components $\sigma_y(b,z)$, $\sigma_{yz}(b,z)$, and $\sigma_{yx}(b,z)$ as reported in reference [4]. The present finite difference predictions show that $\sigma_y(b,z)$, $\sigma_{yx}(b,z)$ are identically zero everywhere along the free edge except at the interface corner, and that $\sigma_{yz}(b,z)$ is zero everywhere, including the interface corner. It should be noted that $\sigma_y(b,z)$, $\sigma_{yx}(b,z)$, and $\sigma_{yz}(b,z)$ are required by the finite difference method to be zero at all grid points along $y = b$ except the grid point that coincides with the interface corner. Thus, the values for these latter stress components that are shown in the figures are calculated from the stress-strain relations and may not represent boundary values. That is the stress tensor may not be symmetrical at the interface corner.

It is known that at a singular point all stress components are either zero or are singular with the same power. The finite difference solution presented here appears to satisfy this criterion.

Case II. $\sigma_{yu} = \sigma_{yxu} = \sigma_{yzu} = 0$ at The Interface Corner. The Case II finite difference solution differs from the principal finite difference solution only in the boundary conditions applied at the grid point that coincides with the interface corner. Accordingly, interlaminar stress continuity at the interface corner is replaced by specifying that $\sigma_{yu}(b,h) = \sigma_{yxu}(b,h) = \sigma_{yzu}(b,h) = 0$. That is, the stress components on the free edge that are associated with the upper ply are prescribed to be zero at the interface corner.

Figure 16 shows the finite difference predictions for the distributions of the interlaminar stress components along the interface. This figure shows that discontinuities in the normal stress σ_z and the shearing stress σ_{zx} occur at the interface corner. Otherwise, continuity of the interlaminar group is maintained along the interface.

Figure 17 shows the finite difference predictions for the distributions of the in-plane group of stress components along the interface for the upper and lower plies. An important observation to make from the curves in Figure 17 is that each stress component associated with the lower ply ($\sigma_{x\ell}$, $\sigma_{y\ell}$, $\sigma_{xy\ell}$) behaves as if a stress singularity existed at the interface corner, while each stress component associated with the upper ply (σ_{xu}, σ_{yu} σ_{xyu}) shows a sudden and drastic digression from what appears to be a distribution that is trying to follow the corresponding distribution of the lower ply.

The stress distributions associated with the in-plane stresses of the upper ply exhibit behaviors near the interface corner similar to those exhibited by the finite element method.

-16-

Figure 18 shows the distribution of the boundary stresses along the free edge $y = b$. The finite difference method requires $\sigma_{yu}(b,z) = \sigma_{yxu}(b,z) = \sigma_{yzu}(b,z) = 0$ at all grid points in the upper ply, including the interface corner. It requires that $\sigma_{y\ell}(b,z) = \sigma_{yx\ell}(b,z) = \sigma_{yz\ell}(b,z) = 0$ at all grid points in the lower ply, except at the interface corner. Numerical values for $\sigma_{y\ell}(b,h)$, $\sigma_{yx\ell}(b,h)$, and $\sigma_{yz\ell}(b,h)$ calculated from the appropriate stress-strain relations are shown on the figure.

Case III. $\sigma_{y\ell} = \sigma_{yx\ell} = \sigma_{yz\ell} = 0$ at The Interface Corner. The Case III finite difference solution differs from the principal finite difference solution only in the boundary conditions applied at the grid point that coincides with the interface corner. Accordingly, interlaminar stress continuity at the interface corner is replaced by the conditions $\sigma_{y\ell}(b,h) = \sigma_{yx\ell}(b,h) = \sigma_{yz\ell}(b,h) = 0$. That is, the stress components on the free edge that are associated with the lower ply are prescribed to be zero at the interface corner.

Figure 19 shows the finite difference distributions for the interlaminar stress components. The stress component $\sigma_{zy}(y,h)$ is zero everywhere along the interface. This figure shows that discontinuities in the normal stress σ_z and the shearing stress σ_{zx} occur at the interface in exactly the same manner as in Case II.

Figure 20 shows the finite difference predictions for the distributions of the in-plane group of stress components along the interface. An important observation to make from the curves in Figure 20 is that each stress component associated with the upper ply (σ_{xu}, σ_{yu}, σ_{xyu}) behaves as if a stress singularity existed at the interface corner, while each stress component associated with the lower ply ($\sigma_{x\ell}$, $\sigma_{y\ell}$, $\sigma_{xy\ell}$) shows a sudden and drastic digression from what appears to be a distribution that is trying to follow the corresponding distribution of the upper ply.

Figure 21 shows the distributions of the boundary stresses along the free edge $y = b$. The finite difference method requires $\sigma_{y\ell}(b,z) = \sigma_{yx\ell}(b,z) = \sigma_{yz\ell}(b,z) = 0$ at all grid points in the lower ply, including the interface corner. It requires $\sigma_{yu}(b,z) = \sigma_{yxu}(b,z) = \sigma_{yzu}(b,z) = 0$ at all grid points in the upper ply, except at the interface corner. Numerical values for $\sigma_{yu}(b,h)$, $\sigma_{yxu}(b,h)$, and $\sigma_{yzu}(b,h)$ calculated from the appropriate stress-strain relations are shown on the figure.

Case IV. Average Stress Boundary Condition. The Case IV finite difference solution differs from the principal finite difference solution only in the boundary conditions imposed at the grid point that coincides with the interface corner. Accordingly, interlaminar stress continuity at the interface corner is replaced by the conditions $(\sigma_y)_{ave} = (\sigma_{yx})_{ave} = (\sigma_{yz})_{ave} = 0$ at the interface corner. Here $(\sigma)_{ave}$ denotes the average of corresponding stress components for the upper and lower plies.

Figure 22 shows the finite difference distributions for the interlaminar stress components along the interface. The finite difference predictions for the interlaminar stress components (σ_z, σ_{zx}, and σ_{zy}) exhibited in this figure are in excellent agreement in every respect with the finite element predictions for the corresponding stress components.

Figure 23 shows the finite difference predictions for the distributions of the in-plane group of stress components along the interface for the upper and lower plies. An important observation to make from the curves in Figure 23 is that the stress components associated with both the upper ply (σ_{xu}, σ_{xyu}, σ_{yu}) and the lower ply ($\sigma_{x\ell}$, $\sigma_{xy\ell}$, $\sigma_{y\ell}$) each show the curious digressive behavior at the interface corner that characterizes the finite element predictions for these stress components.

The foregoing observations provide a clue to the reason the finite element method behaves in the curious manner described in reference [4] near the

interface corner. The possible reason for the curious behavior is discussed in the conclusions section of this report.

Figure 24 shows the distributions of the boundary stresses along the free edge y = b. The finite difference method requires $\sigma_{yu}(b,z) = \sigma_{yxu}(b,z) = \sigma_{yzu}(b,z) = 0$ at all points in the upper ply, except at the interface corner, and $\sigma_{y\ell}(b,z) = \sigma_{xy\ell}(b,z) = \sigma_{yz\ell}(b,z) = 0$ at all points in the lower ply, except at the interface corner. Numerical values for $\sigma_{yu}(b,h)$, $\sigma_{yxu}(b,h)$ and $\sigma_{yzu}(b,h)$, $\sigma_{y\ell}(b,h)$, $\sigma_{yx\ell}(b,h)$, and $\sigma_{yz\ell}(b,h)$ calculated from appropriate stress-strain relations are shown on the figure. Again, it is noted that these numerical values are not necessarily boundary values because the stress tensor may not be symmetrical at the interface corner.

An interesting feature of the present case is that while continuity of the interlaminar stress components was not enforced directly at the interface corner, continuity of these stresses occurred there nevertheless.

V. CONCLUSIONS

Distributed Load Problem. Both the finite element and finite difference methods predict shearing stress distributions along the line $x = a$ that are in excellent agreement with each other and with the exact solution, except near the point (a,0). The finite difference solution behaves somewhat better than the finite element solution in this region, deviating from the exact solution only to satisfy the imposed boundary condition $\sigma_{yx}(a,0) = 0$. Since the exact solution shows that the stress tensor is not symmetrical at the point (a,0), this deviation from the exact solution cannot be attributed to an inherent weakness of the finite difference method. The trouble arises because of the need to specify a limiting value for $\sigma_{xy}(a,0)$ at a point where $\sigma_{xy} \neq \sigma_{yx}$.

Bimetallic Plate Problem. The finite difference and the finite element methods predict essentially the same shearing stress distribution along the bond line. It is interesting to observe that the displacement components are prescribed along the bond line, including the singular point. Consequently, no finite difference boundary conditions are prescribed for σ_x and σ_{xy} at the grid point that coincides with the singular point. Numerical values for σ_x and σ_{yx} at the singular point are calculated from the stress-strain relations and are not necessarily boundary values since the stress tensor may not be symmetrical there.

Four-Ply Laminate. Based on the numerical evidence presented in the principal finite difference solution for the four-ply laminate under uniform axial strain it appears that there is no inherent weakness in the finite difference method that prevents it from providing accurate predictions for the distributions of the interlaminar stress group and for

the in-plane stress group along the interface, except very near the interface corner. And, even near the interface corner, the finite difference method provides solutions that behave in a way that is characteristic of the behavior of stresses near a singular point.

The four finite difference solutions for the stress distributions associated with the interlaminar stress group (σ_z, σ_{zx}, σ_{zy}) and the in-plane stress group (σ_x, σ_y, σ_{xy}) differ only near the interface corner. This is not unexpected, since the finite difference models for the four solutions differ only in the boundary conditions imposed at a single boundary point—boundary conditions that are, moreover, very similar.

Of the four finite difference solutions the stress distributions predicted by the Case I model (stress continuity along the interface) behave near the interface corner as one expects them to behave near a stress singularity. Therefore, it is felt that the Case I predictions should be the definitive solution.

The Case II and III models exhibit behaviors that are similar near the interface corner. That is, discontinuities appear in the interlaminar stress components σ_z and σ_{zx}, and corresponding in-plane stress components for the + 45 ply and the − 45 ply show divergent behaviors near the interface corners. Specifically, for the Case II model the in-plane stress components for the + 45 ply are "drawn" down to satisfy the boundary conditions imposed at the interface corner, while the in-plane stress components for the −45 ply appear to grow unboundedly. Just the reverse is true for the Case III finite difference model.

Stress distributions predicted by the Case IV finite difference model agree extremely well, in all respects, with the finite element predictions of the same distributions. Consequently, one is led to examine the boundary conditions imposed by the two models at the interface corner to explain the curious behavior exhibited there by the finite element model.

Consider two finite elements, located at the interface corner, which
share the interface corner as a common node. Let one side of each element lie
on the free edge. The finite element procedure replaces a distributed load on
an element boundary with concentrated forces acting at the nodes of the element.
Statical equivalency between the distributed boundary load and the concentrated
nodal forces is maintained by requiring the virtual work of the nodal forces on
the corresponding nodal displacements be equal to the virtual work of the actual
boundary load distribution on the displacements along the boundary to which
the load is applied. Therefore, the finite element node coincident with the
interface corner receives "average" contributions from the finite elements on
either side of the interface. In a finite element solution a stress-free boundary
condition translates into a nodal force-free boundary condition. Therefore,
setting the nodal force at the interface corner equal to zero is, in some
sense, an averaging procedure similar to the boundary conditions used in the
Case IV model. It is this "averaging" process that apparently eliminates the
detail that an accurate solution near the interface corner requires.

REFERENCES

1. R. Byron Pipes and N. J. Pagano, Interlaminar stresses in composite laminates under uniform axial extension. J. Compos. Mater. 4, 538-548, (1970).

2. Peter W. Hsu and Carl T. Herakovich, Edge effects in angle-ply composite laminates. J. Compos. Mater. 11, 422-428, (1977).

3. S. S. Wang and R. J. Stango, Optimally discretized finite elements for boundary layer stresses in composite laminates, 23rd Structures, Structural Dynamics, and Materials Conference, Part I, 328-337, (1982).

4. J. D. Whitcomb, I. S. Raju, and J. G. Goree, Reliability of the finite-element method for calculating free edge stresses in composite laminates, International Journal of Computers and Structures. Vol. 4, No. 1, 28-37, (1982).

Table I. Finite difference grid spacings for the distributed load on a semi-infinite plate. Finite difference grid contained 29 rows and 37 columns (2146 degrees of freedom).

Number of spaces	First 2	Next 4	Next 1	Next 12	Next 1	Next 4	Next 2	Next 2	Next 2	Next 2	Next 2	Next 2
x-spacing	0.20	0.10	0.05	0.025	0.05	0.10	0.20	0.25	0.50	0.75	1.00	1.50

Number of spaces	First 8	Next 4	Next 2	Next 2	Next 2	Next 2	Next 2	Next 6
y-spacing	0.025	0.05	0.10	0.20	0.25	0.50	0.75	1.00

Table II. Finite difference grid spacings for the bimetallic plate loaded by uniform tension. Finite difference grid contained 45 rows and 26 columns (2340 degrees of freedom).

Number of spaces	First 4	Next 6	Next 4	Next 4	Next 4	Next 3
x-spacing	0.025	0.05	0.10	0.20	0.30	0.40

Number of spaces	First 8	Next 8	Next 8	Next 5	Next 4	Next 11
y-spacing	0.025	0.05	0.10	0.20	0.30	0.40

Table III. Locally refined finite difference grid for the bimetallic plate loaded by uniform tension. Finite difference grid contained 45 rows and 26 columns (2340 degrees of freedom).

Number of spaces	First 5	Next 2	Next 3	Next 6	Next 2	Next 2	Next 2	Next 3
x-spacing	0.001	0.010	0.025	0.050	0.10	0.20	0.30	0.8

Number of spaces	First 5	Next 2	Next 7	Next 8	Next 4	Next 4	Next 4	Next 10
y-spacing	0.001	0.010	0.025	0.050	0.10	0.20	0.30	0.50

Table IV. Finite-difference grid spacings for the
four-ply laminate. The grid contained 17 rows and
39 columns (1989 degrees of freedom)

Number of spaces	First 16	Next 2	Next 4	Next 16
y-spacing	1.00	0.50	0.25	0.125

Number of spaces	First 4	Next 8	Next 4
z-spacing	0.20	0.05	0.20

p

a

a

x

y
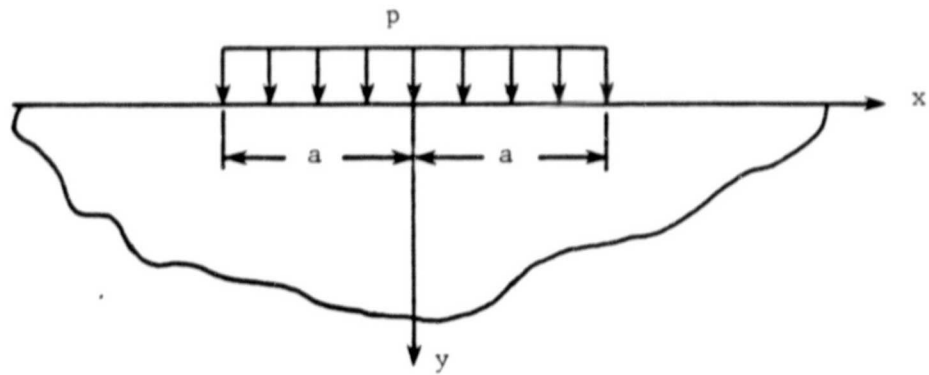
(a) Uniform load on part of a semi-infinite plate.

$$v,_y + \nu u,_x = \frac{-p(1-\nu^2)}{E}$$
$$u,_y + v,_x = 0$$

$$v,_y + \nu u,_x = 0$$
$$u,_y + v,_x = 0$$

a

p

0

x

$$u = 0$$
$$v,_x = 0$$

$$u,_x + \nu v,_y = 0$$

10a

m

$$i-i,$$
$$j+1$$ i, j+1 $$i+1,$$
$$j+1$$

$$\ell$$ i-1,j i,j i+1,j $$u,_y + v,_x = 0$$

$$i-,j-1$$ i,j-1 $$i+1,$$
$$j-1$$

h k

$$v=0$$
$$u,_y + v,_x = 0$$

u,v=0

10a

y
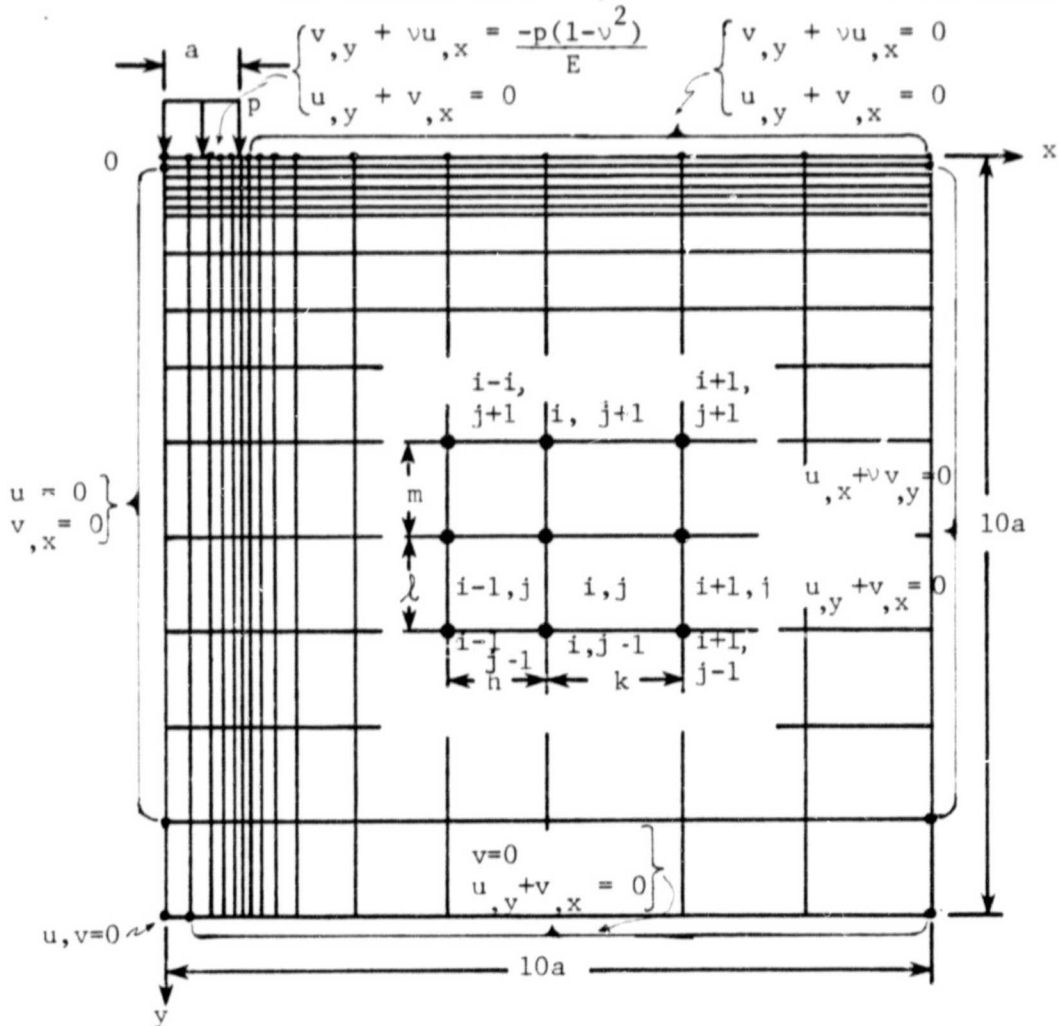
(b) Variable spacing finite - difference grid

Figure 1. Problem involving stress discontinuity
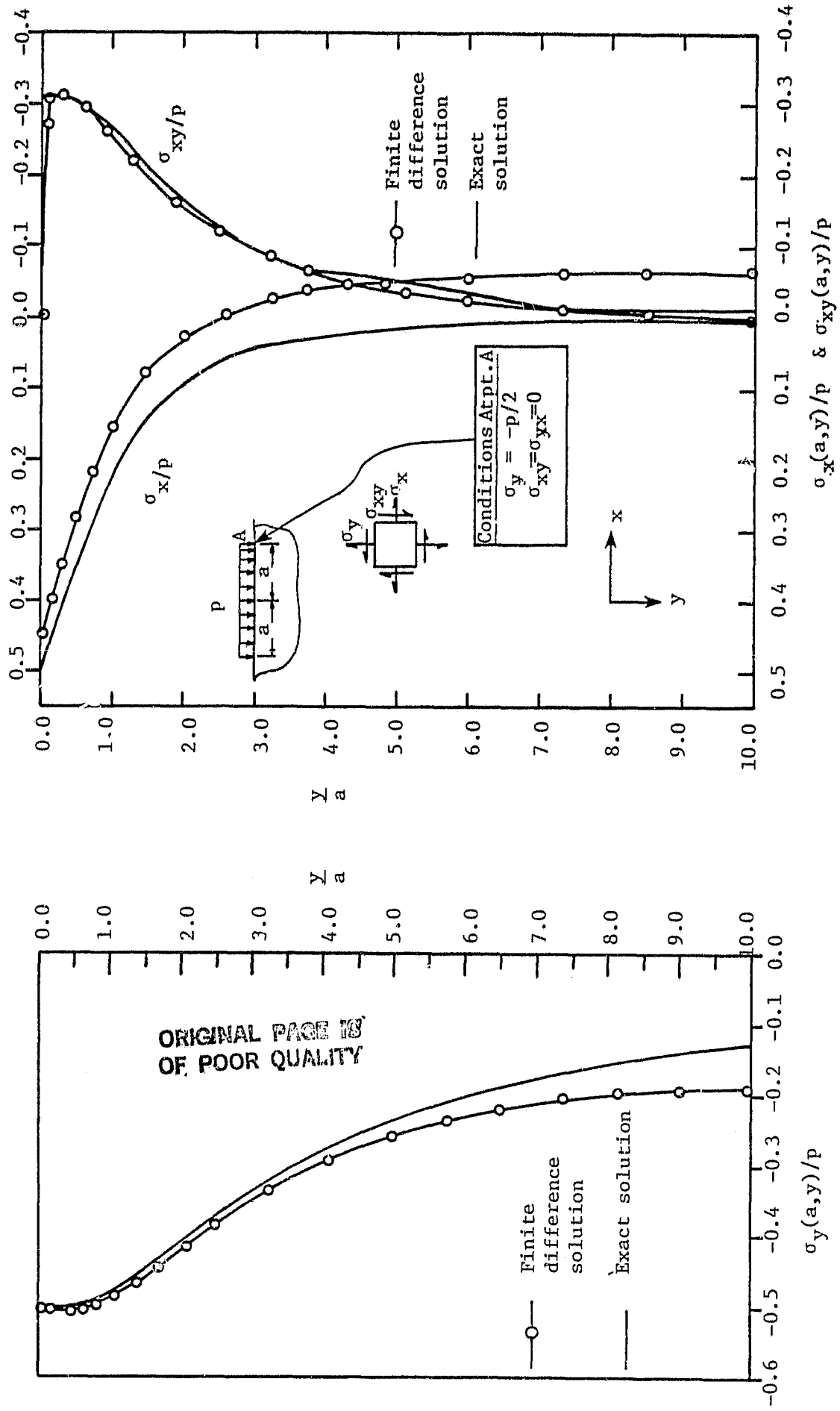
Figure 2. Comparison of finite difference and exact solutions for $\sigma_x(a,y)$, $\sigma_y(a,y)$, and $\sigma_{xy}(a,y)$ for a partially loaded, semi-infinite plate.

-27-

ORIGINAL PAGE IS
OF POOR QUALITY
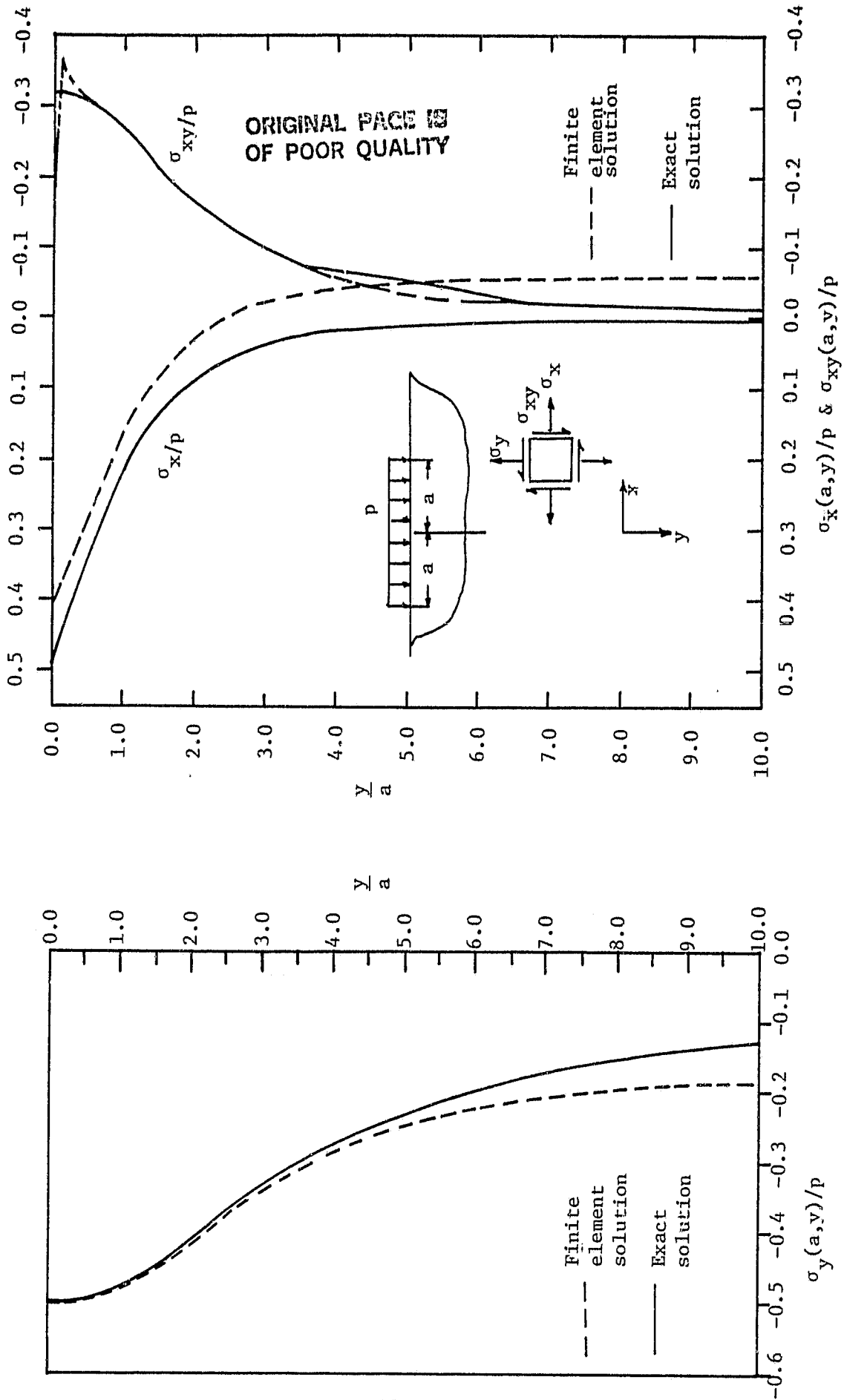
Figure 3. Comparison of finite element and exact solutions for $\sigma_x(a,y)$, $\sigma_y(a,y)$, and $\sigma_{xy}(a,y)$ for partially loaded, semi-infinite plate

(a)

$$\sigma_{xy}(a,y)/p$$

(b)

$$\sigma_x(a,y)/p$$
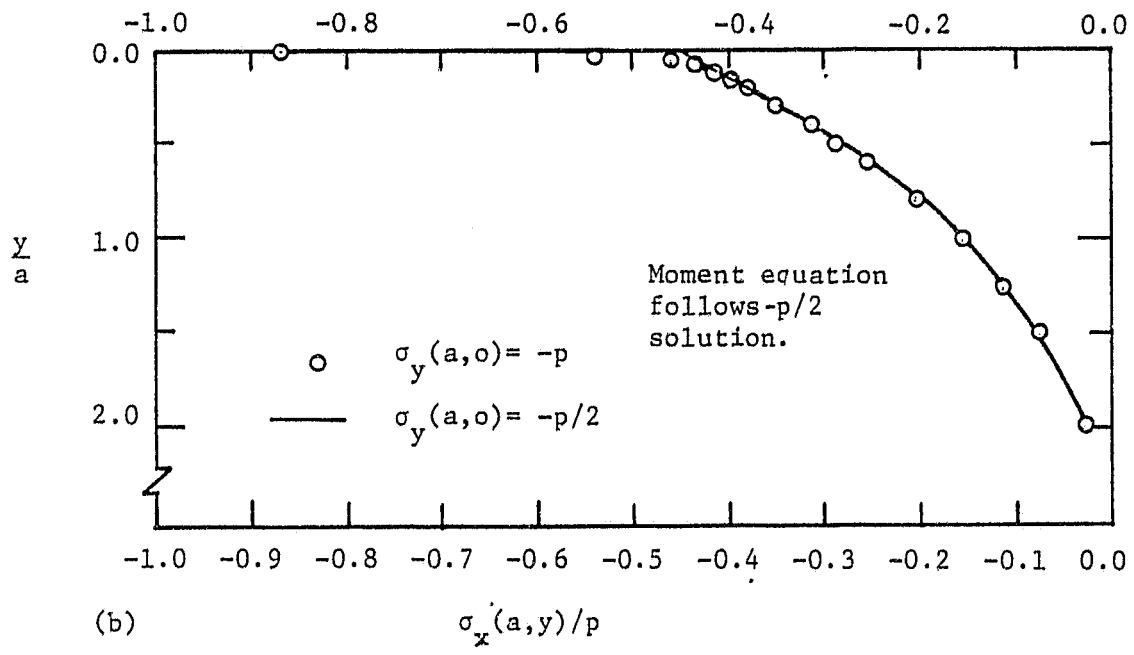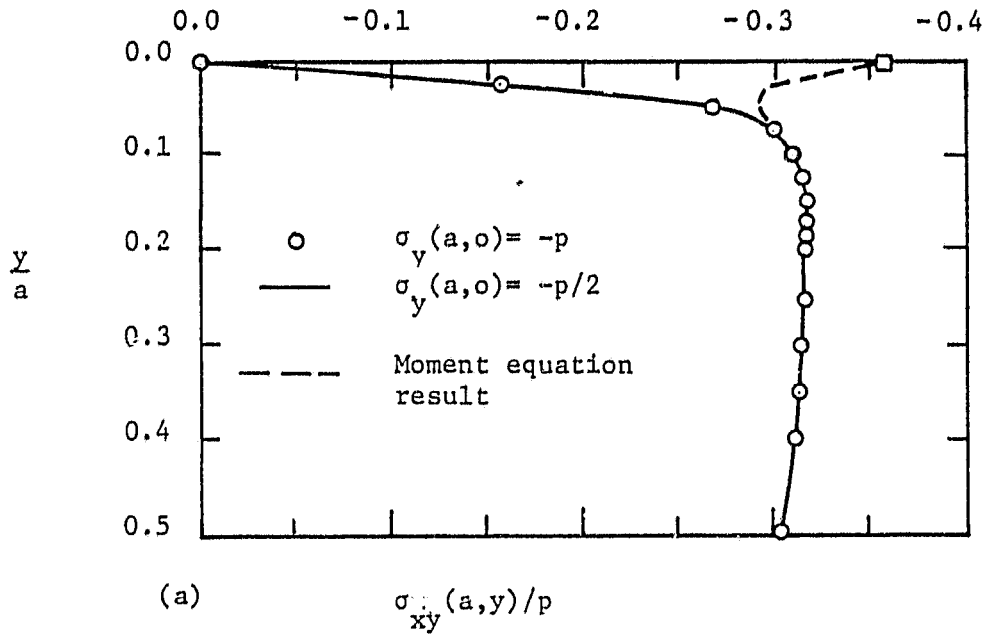
Figure 4. Comparison between $\sigma_x(a,y)$, $\sigma_y(a,y)$, and $\sigma_{xy}(a,y)$
for various boundary conditions at the point (a,o)
and the special moment equation procedure.

(b)

(c)

$$\sigma_{y}(a,y)/p$$
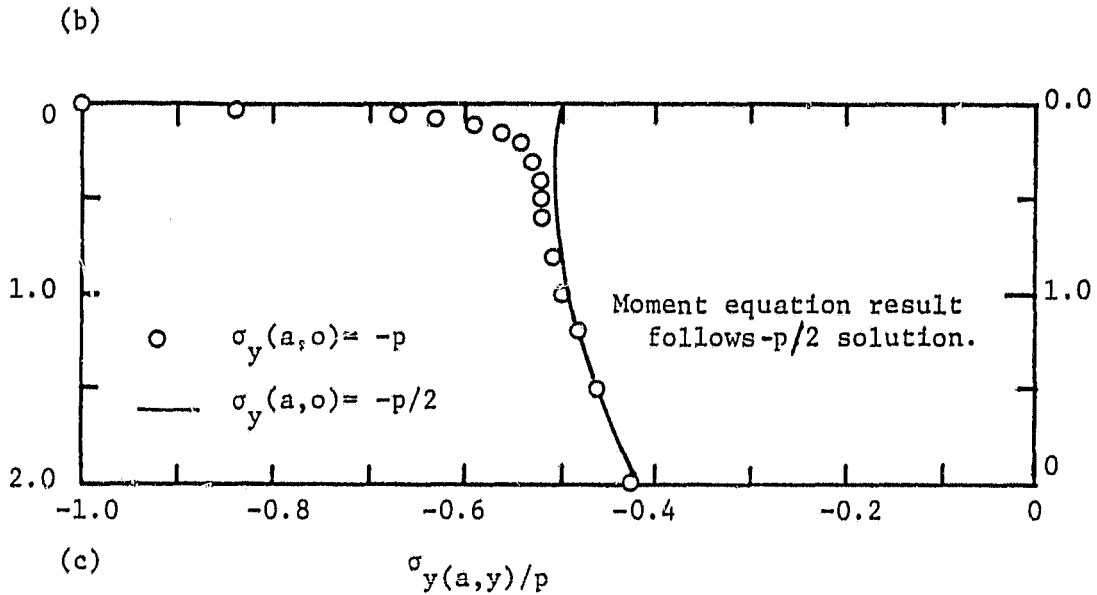
Figure 4 (continued) Comparison between $\sigma_{x}(a,y)$, $\sigma_{y}(a,y)$,

and $\sigma_{xy}(a,y)$ for various boundary conditions at the point

(a,o) and the special moment equation procedure.

(a) An isotropic bimetallic plate under tension.
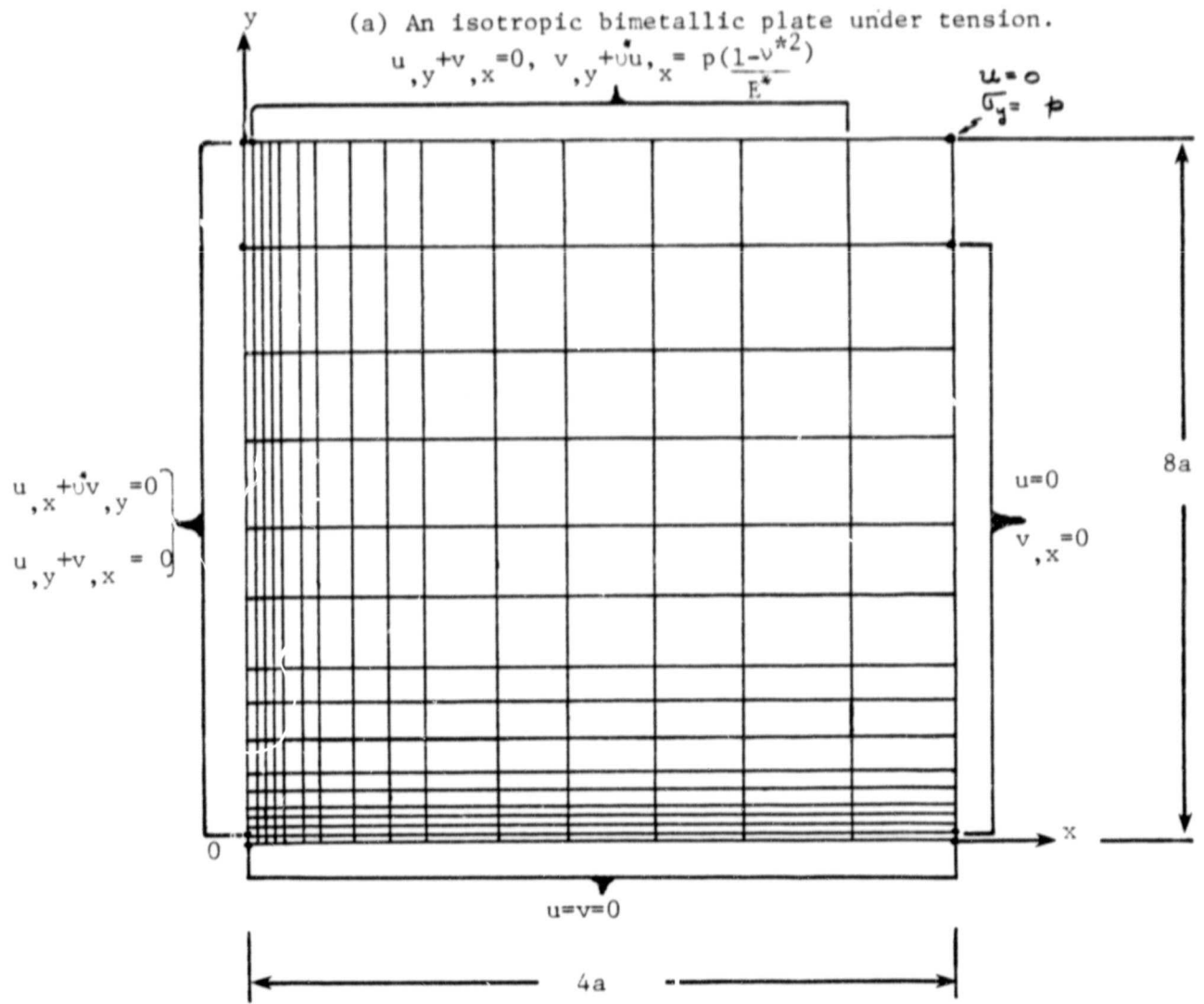
(b) Variable spacing finite difference grid.

Figure 5.   Problem involving a stress singularity.
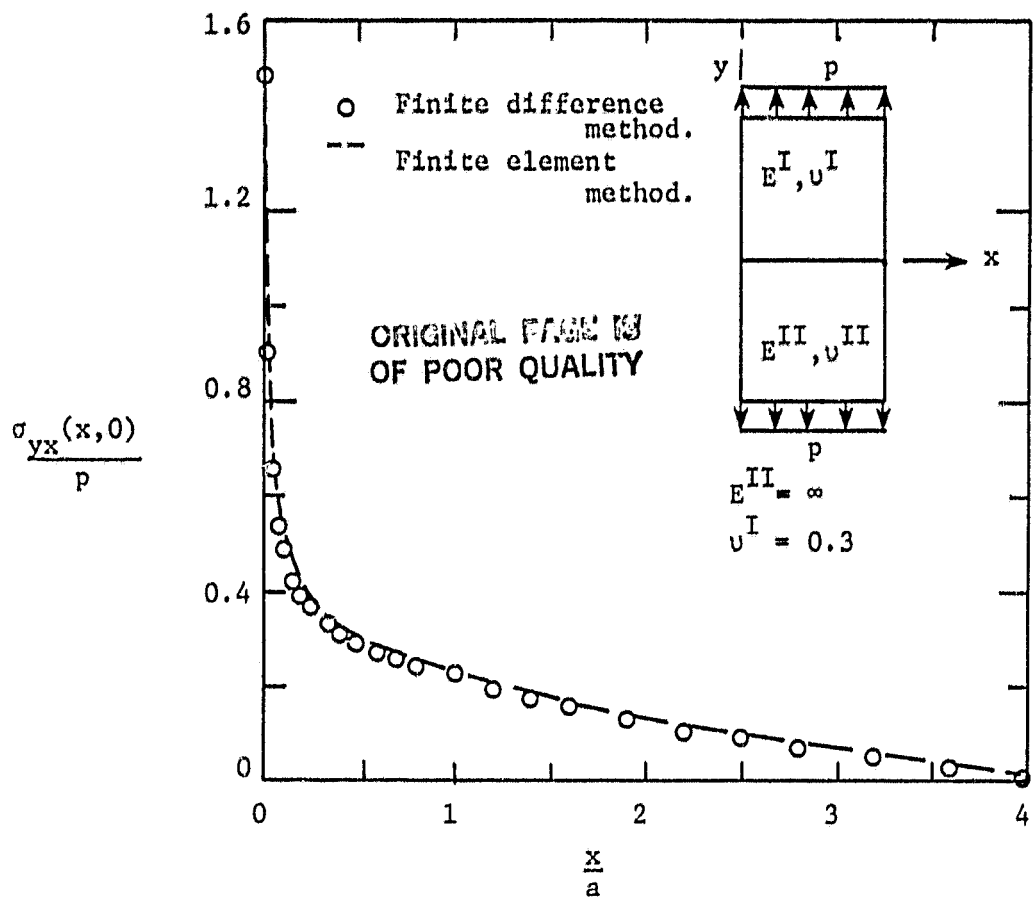
(a) Shear stress (σ_{yx}/p) distribution along the bond line $(y=0)$.
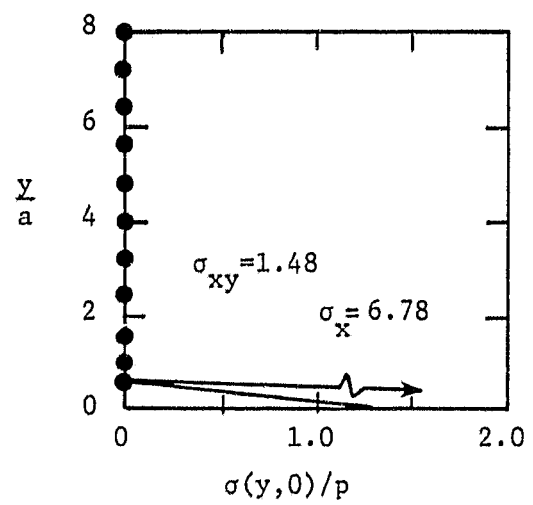
(b) Stress distributions $(\sigma_{xy}/p$ and $\sigma_x/p)$ along the line x=0.

Figure 6. Comparison of finite difference and finite element solutions for the bimetallic plate problem.

Figure 7. Comparison of shearing stress (σ_{xy}/p) distribution along the bond line for two finite difference grids.

(a) Four-ply laminate

(b) 3-D stress components

Figure 8. Laminate configuration, loading, and stresses.

$\sigma_z, \sigma_{zx},$ and σ_{zy} are required to be continuous across the interface except at left interface corner.

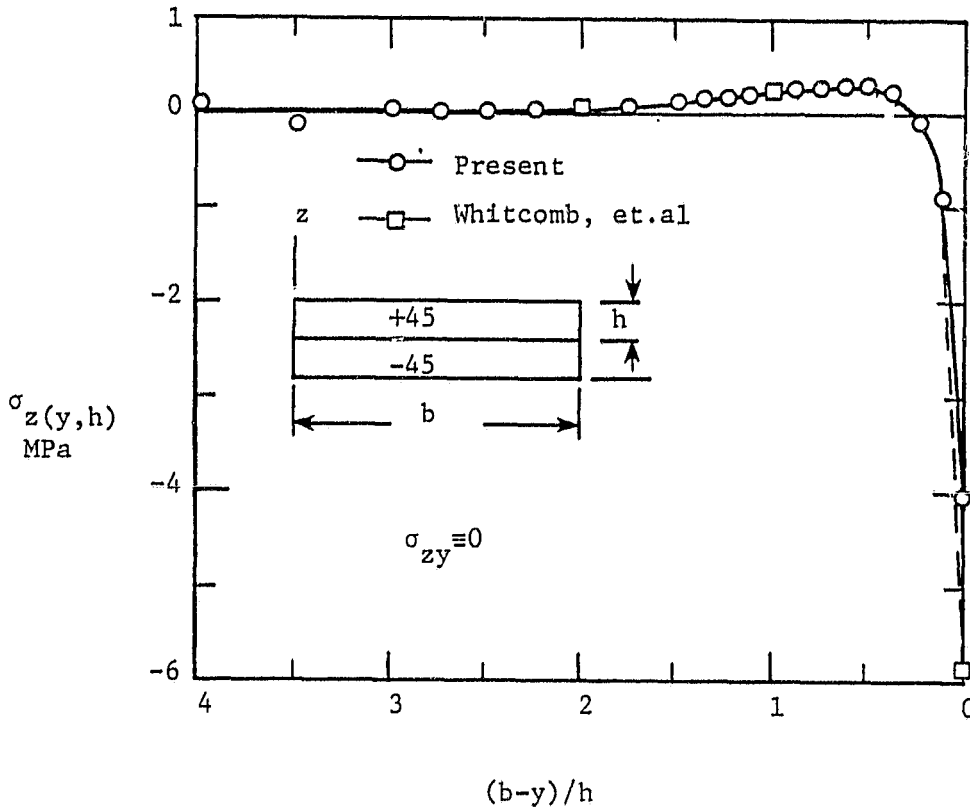Figure 9. Variable spacing finite-difference grid for the four-ply laminate.
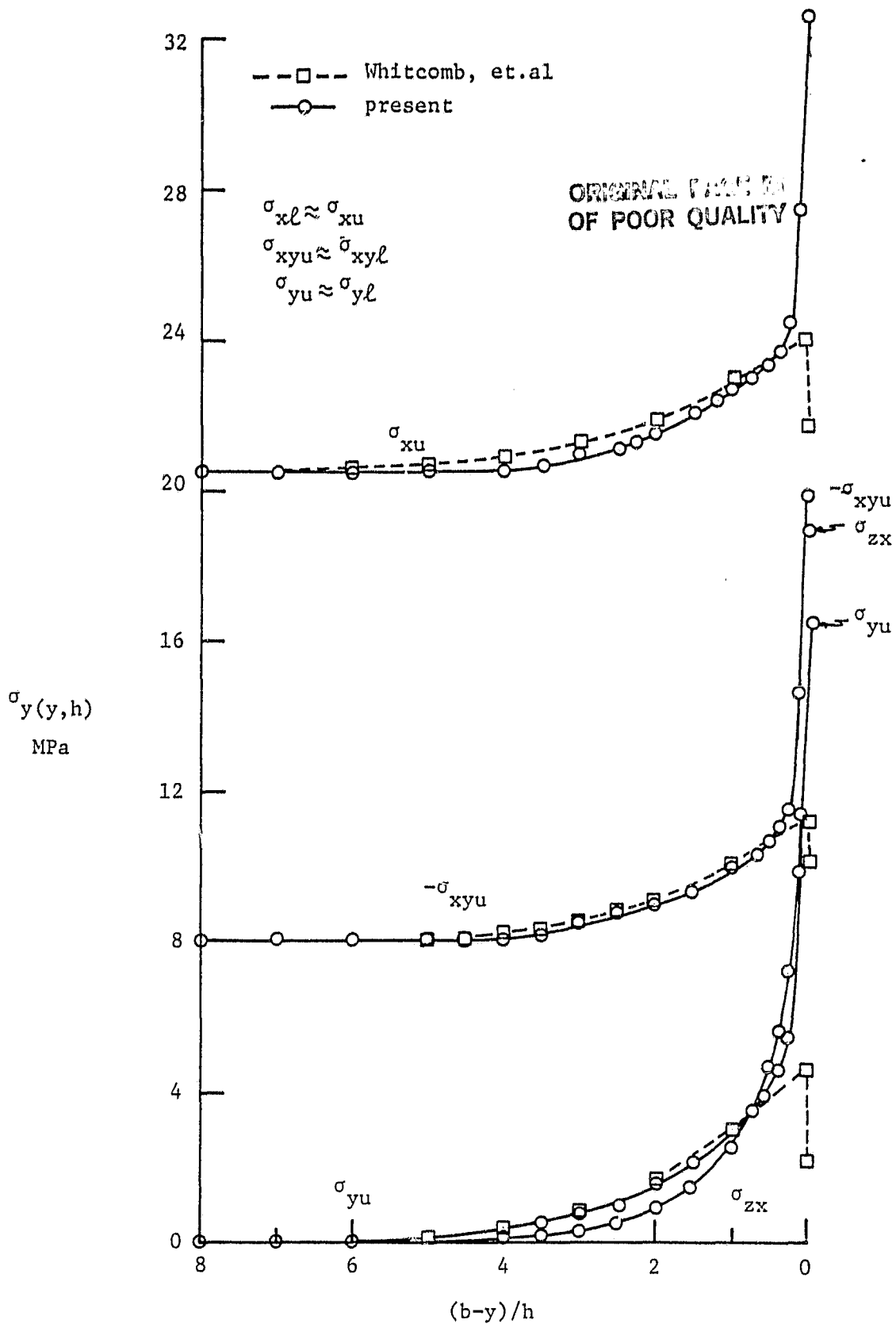
Figure 10. σ_z along the interface, z=h.

Figure 11. Stress distribution along the interface when interlaminar stress continuity is required at every point along the interface, including the interface corner.
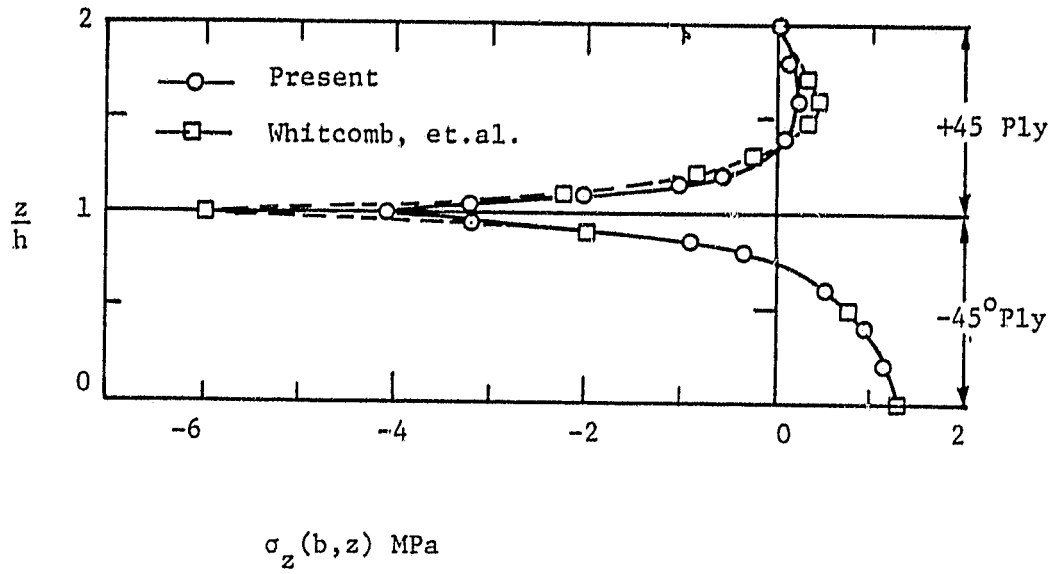
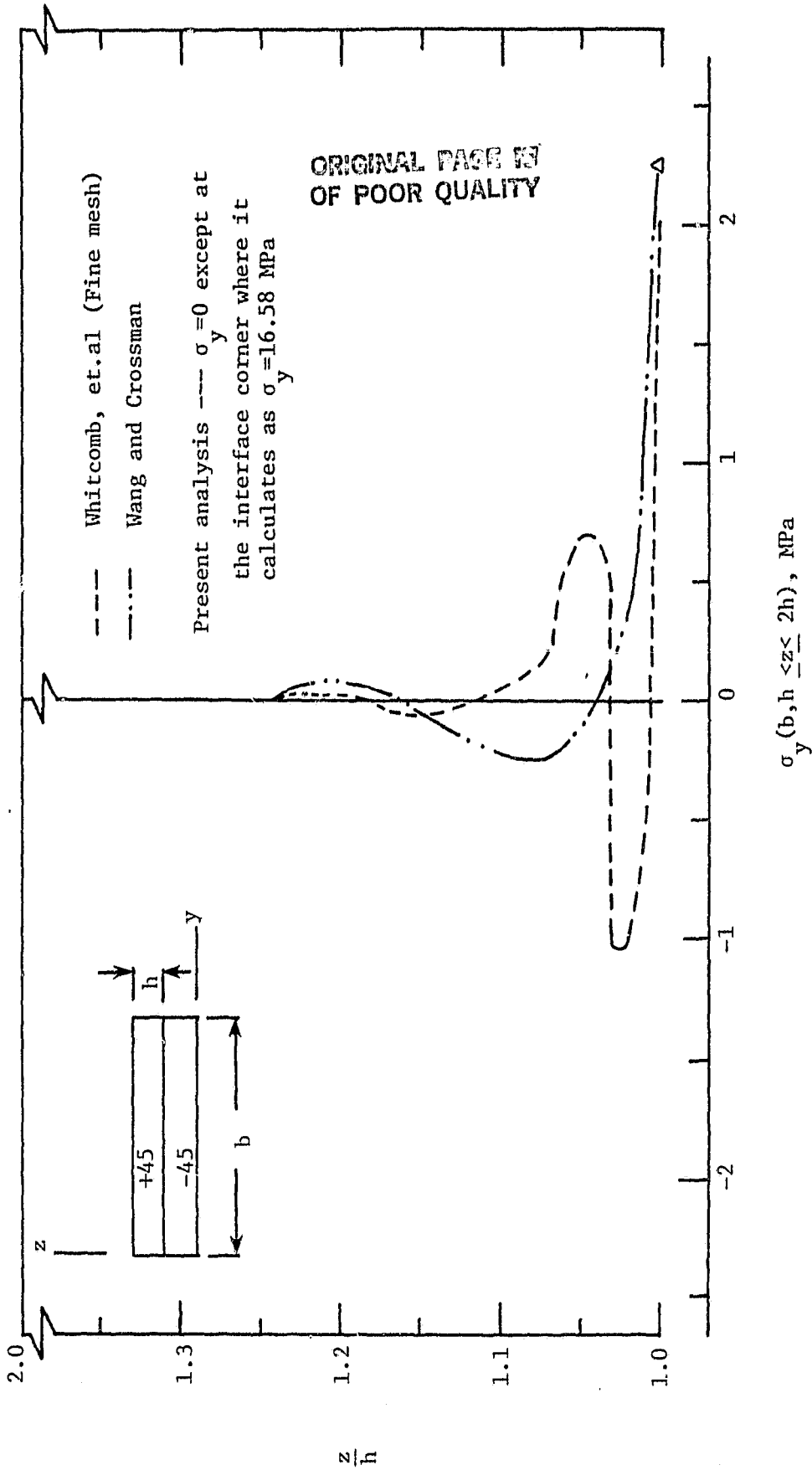Figure 12. σ_z Along the free edge, y=b

Figure 13. Distribution of σ_y through the thickness at the free edge in the $+45°$ ply.
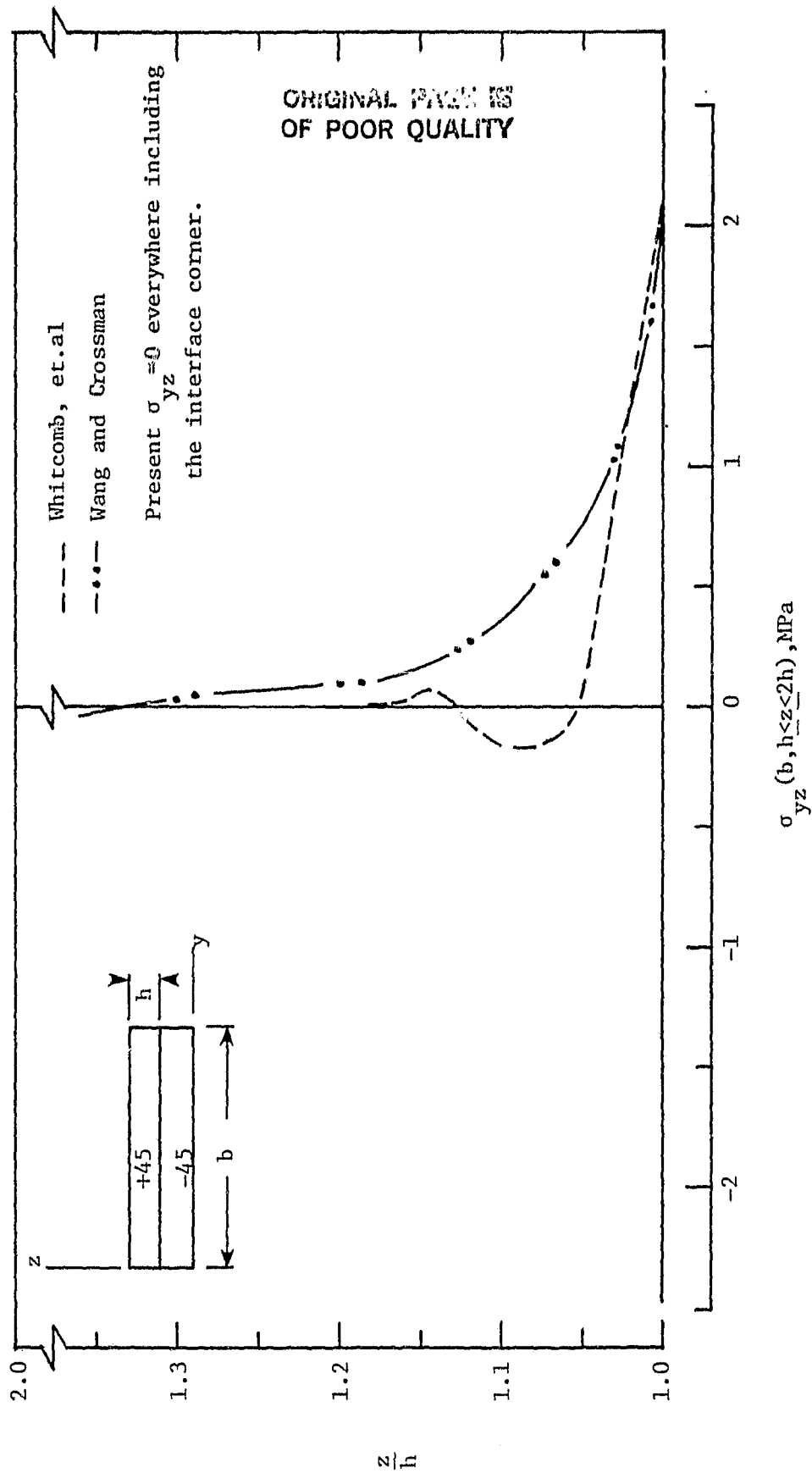
Figure 14. Distribution of σ_{yz} through the thickness at the free edge in the +45 degree ply.
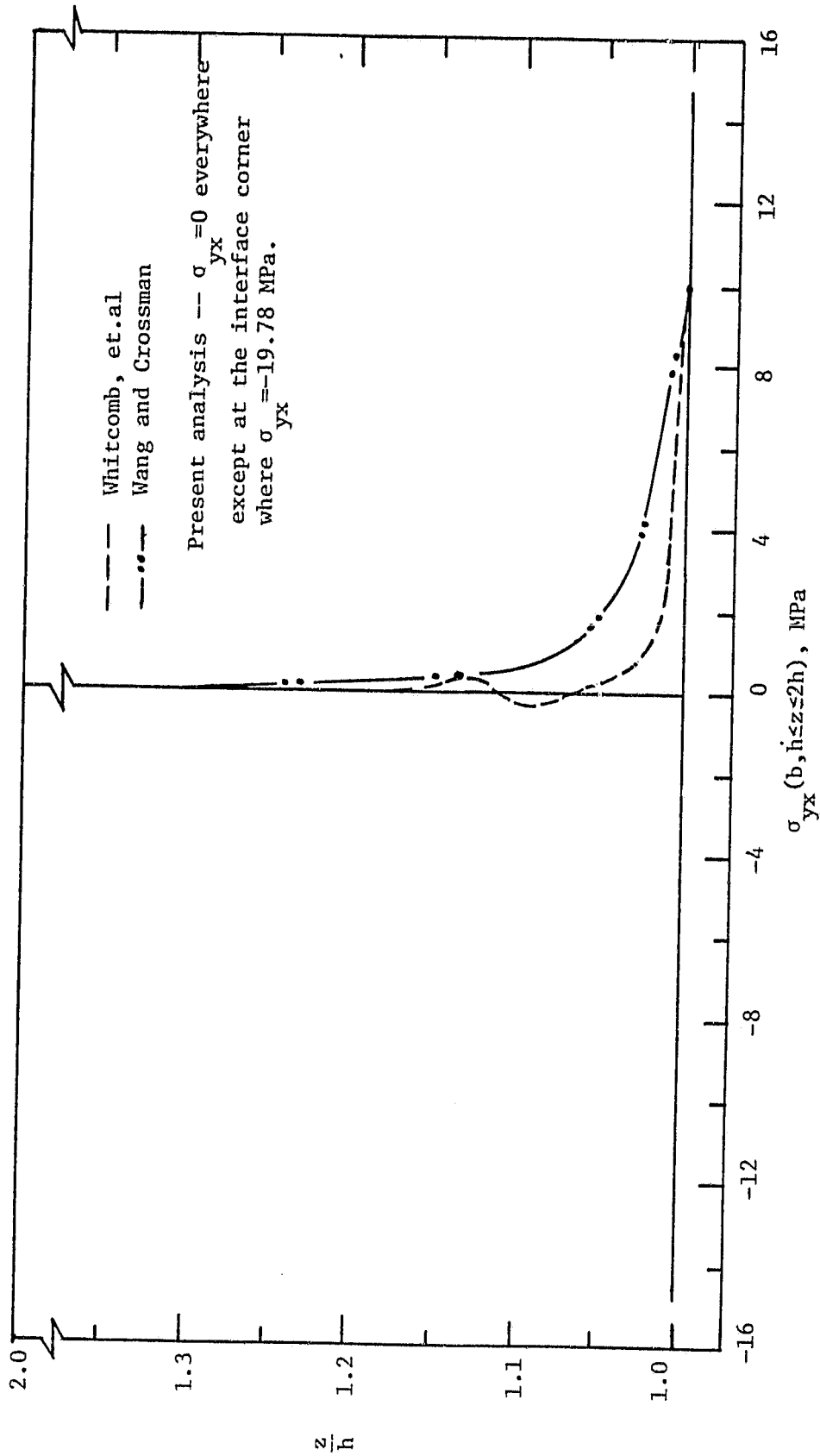
Figure 15. Distribution of σ_{yx} through the thickenss at the free edge in the +45° ply.
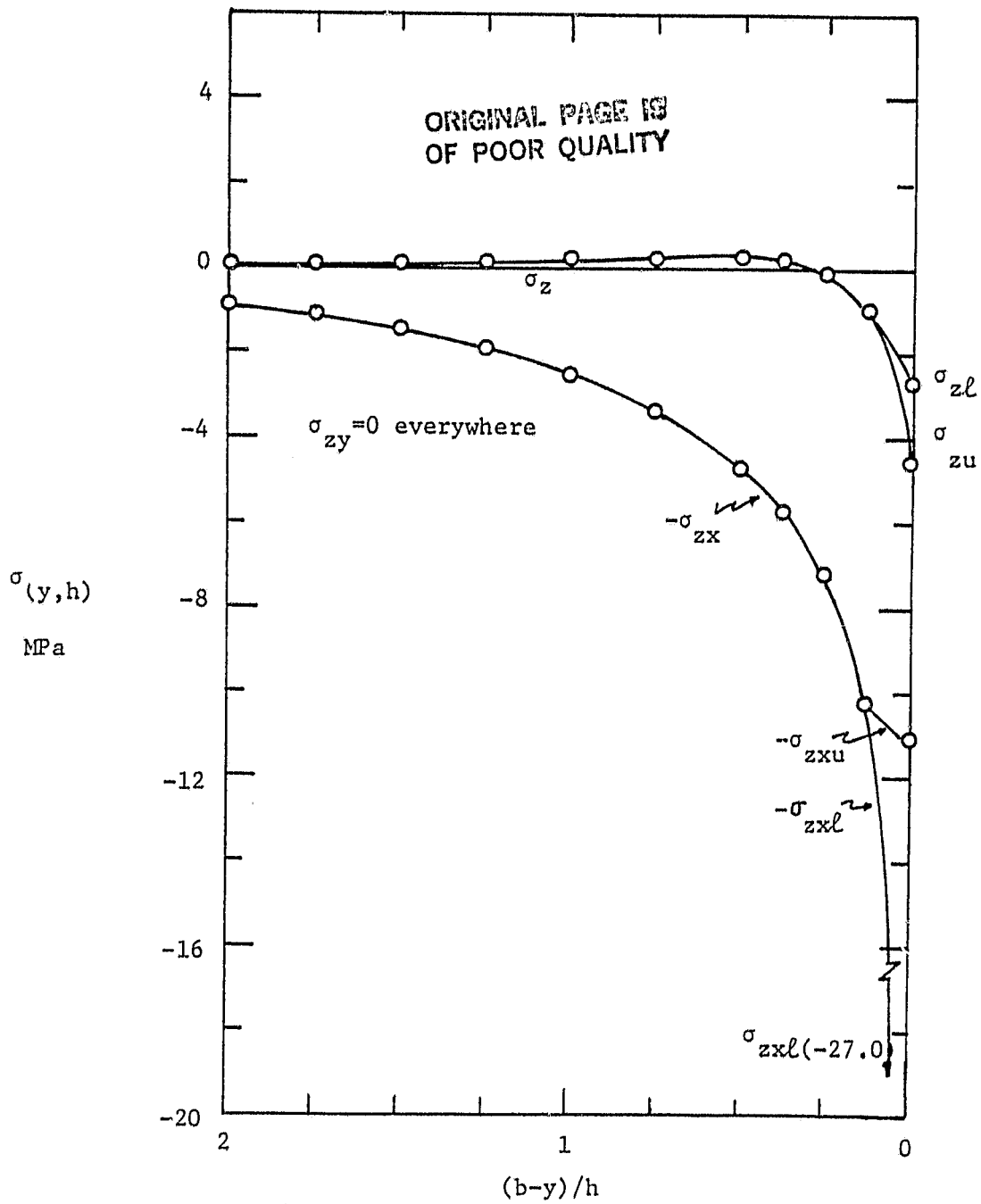
Figure 16. Stress distributions for the interlaminar stress group for $\sigma_{yu} = \sigma_{yxu} = \sigma_{yzu} = 0$ at the interface corner.
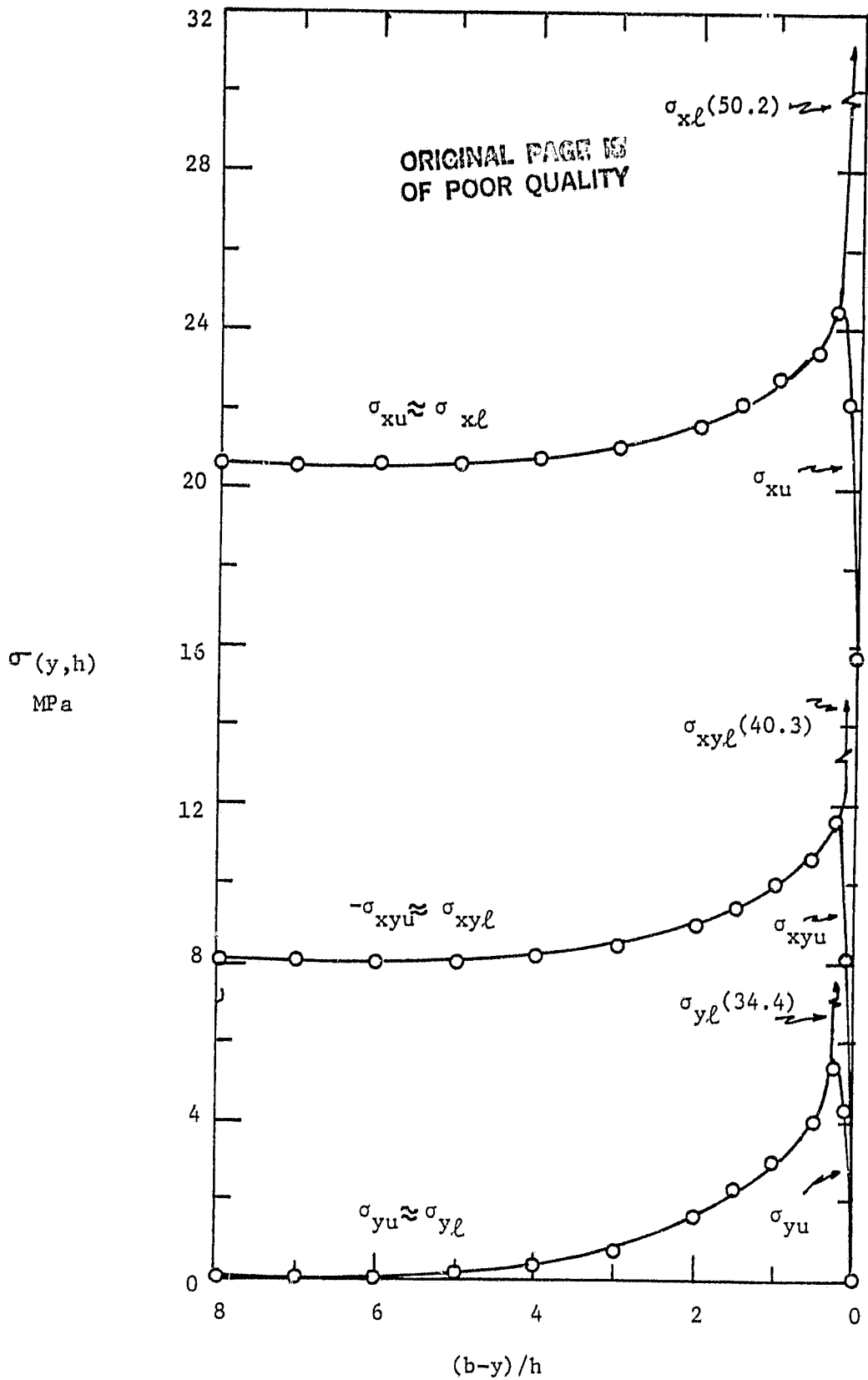
Figure 17. Stress distributions for the in-plane stress group for $\sigma_{yu} = \sigma_{yxu} = \sigma_{yzu} = 0$ at the interface corner.

Figure 18. Stress distributions along the boundary $y=b$ for $\sigma_{yu}=\sigma_{yxu}=\sigma_{yzu}=0$ at the interface corner.

Figure 19. Stress distributions for the interlaminar stress group for $\sigma_{y\ell} = \sigma_{yx\ell} = \sigma_{yz\ell} = 0$ at the interface corner.
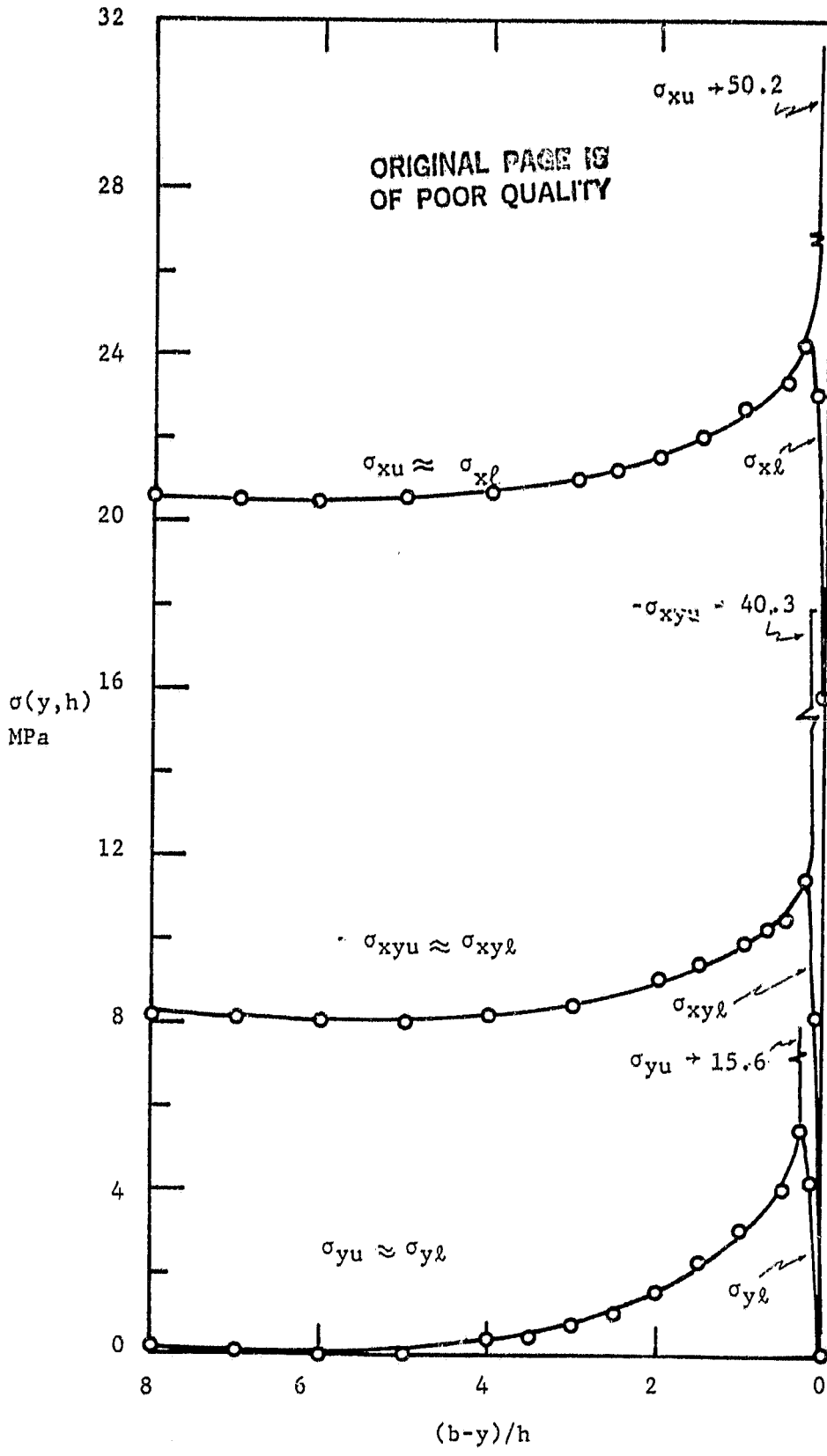
Figure 20. Stress distributions for the in-plane stress group for $\sigma_{y\ell} = \sigma_{yx\ell} = \sigma_{yz\ell} = 0$ at the interface corner.
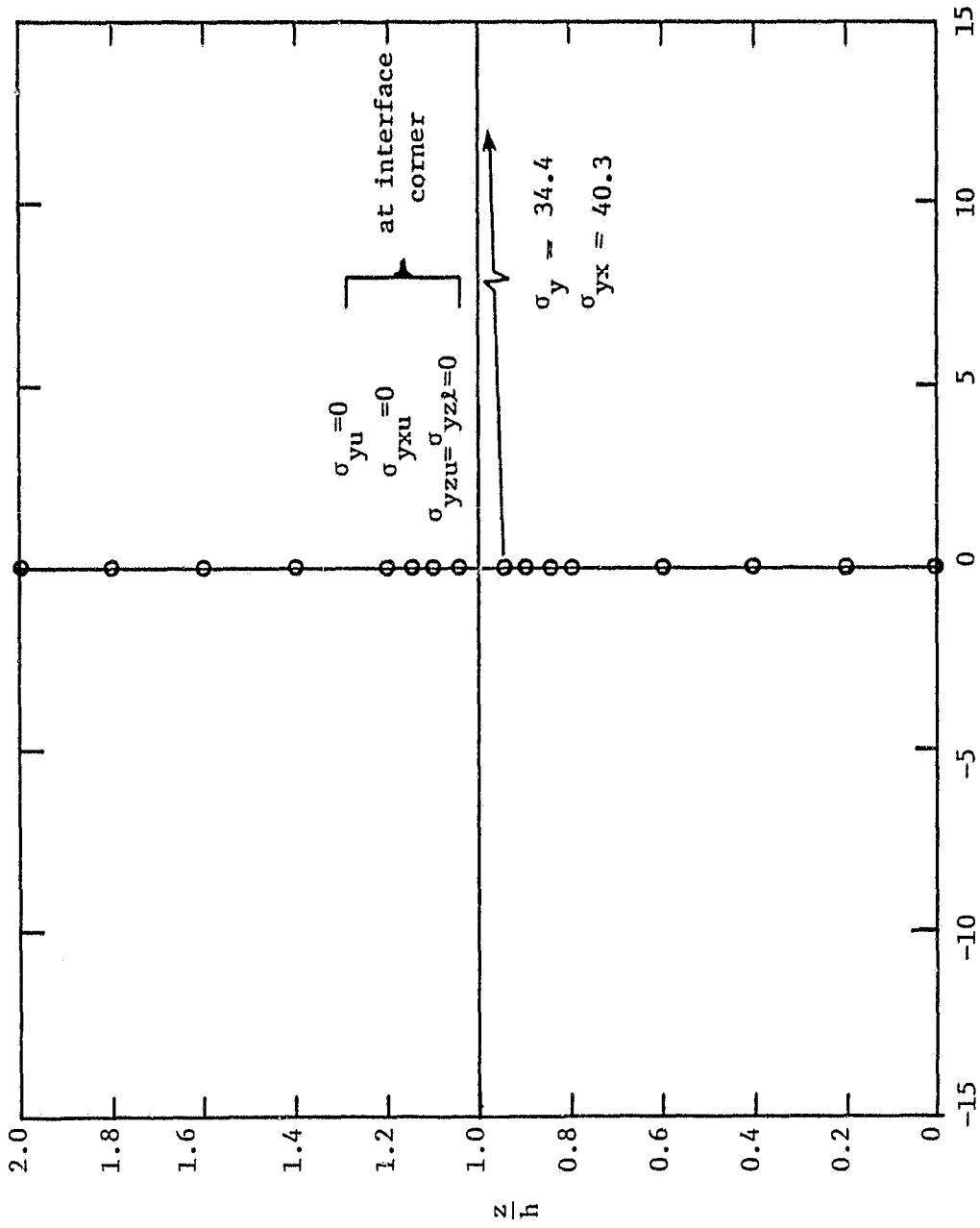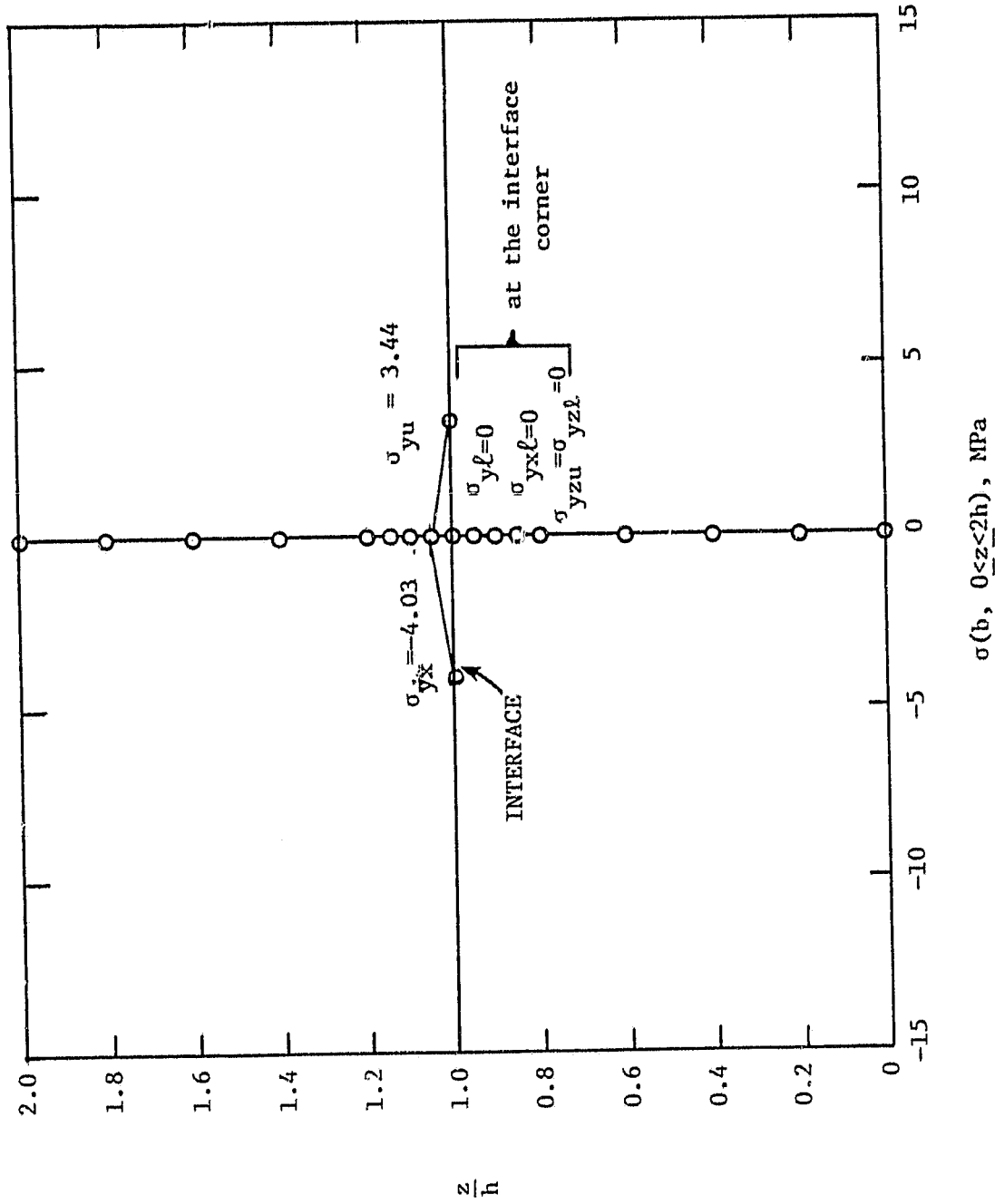
Figure 21. Stress distributions along the boundary $y=b$ for $\sigma_{y\ell}=\sigma_{yx\ell}=\sigma_{yz\ell}=0$ at the interface corner.

-47-

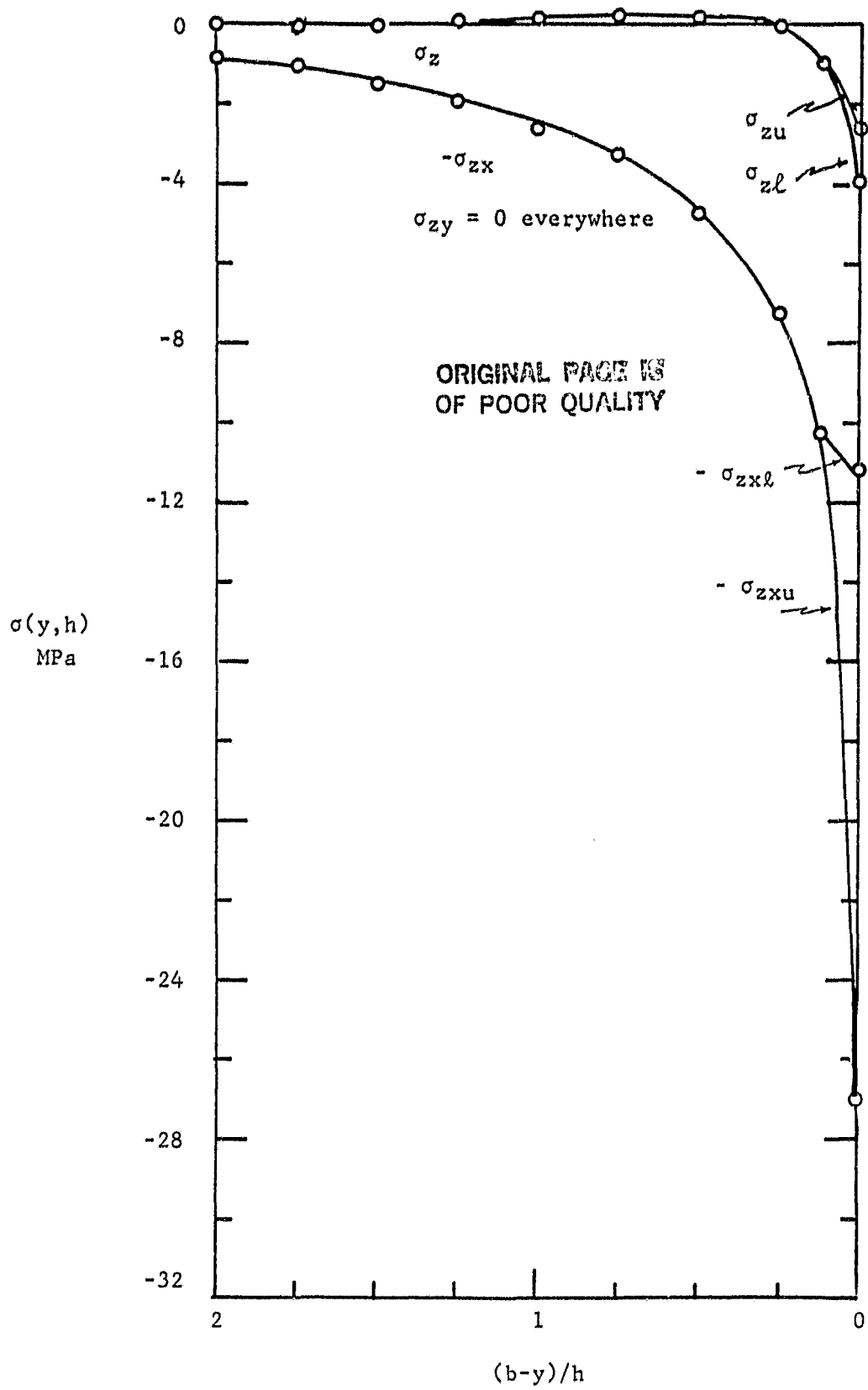Figure 22. Stress distributions for the interlaminar stress group for (σ_y) ave $= (\sigma_{yx})$ ave $= (\sigma_{yz})$ ave $= 0$ at the interface corner.

Figure 23. Stress distributions for the in-plane stress group for (σ_y) ave $= (\sigma_{yx})$ ave $= (\sigma_{yz})$ ave $= 0$ at the interface corner.
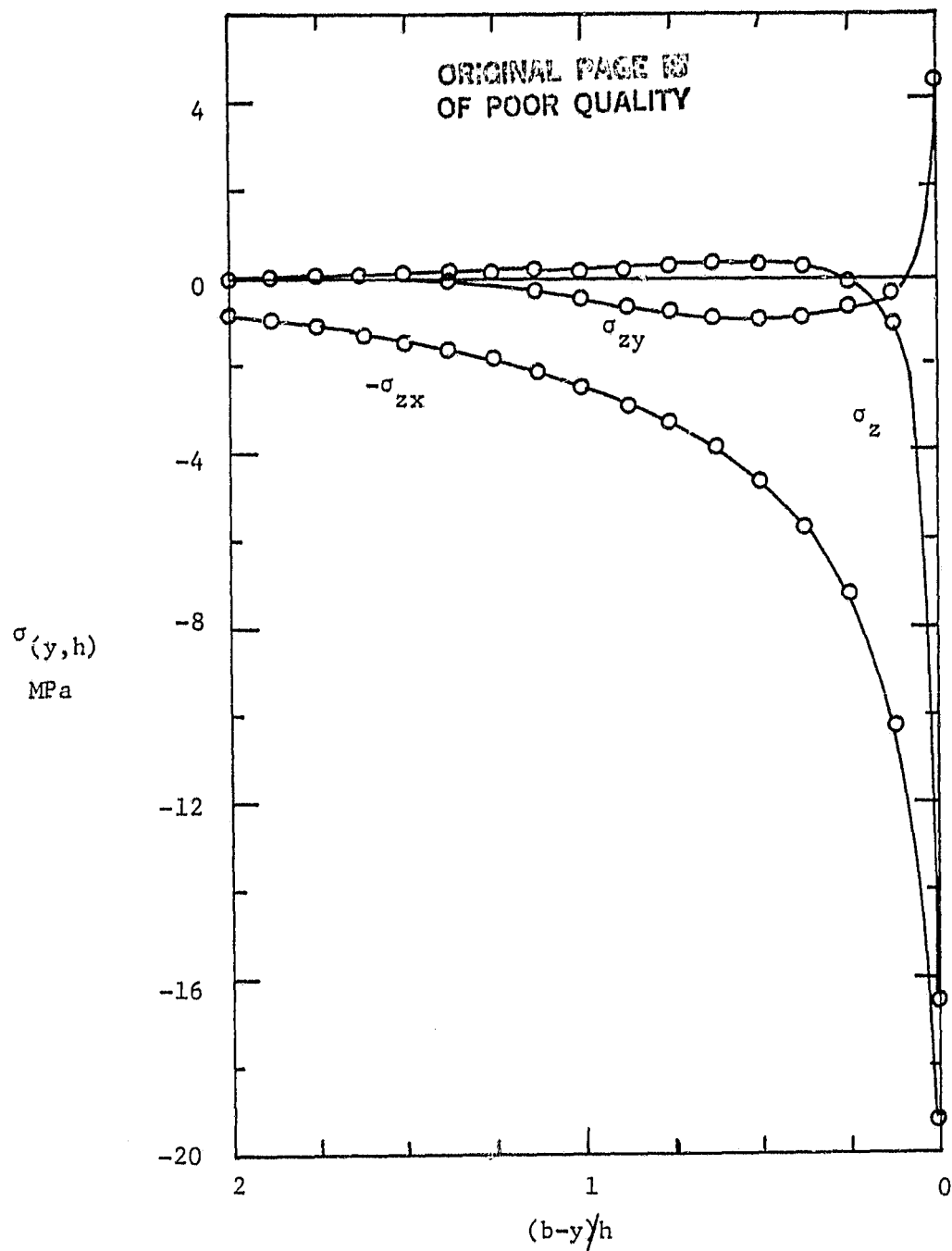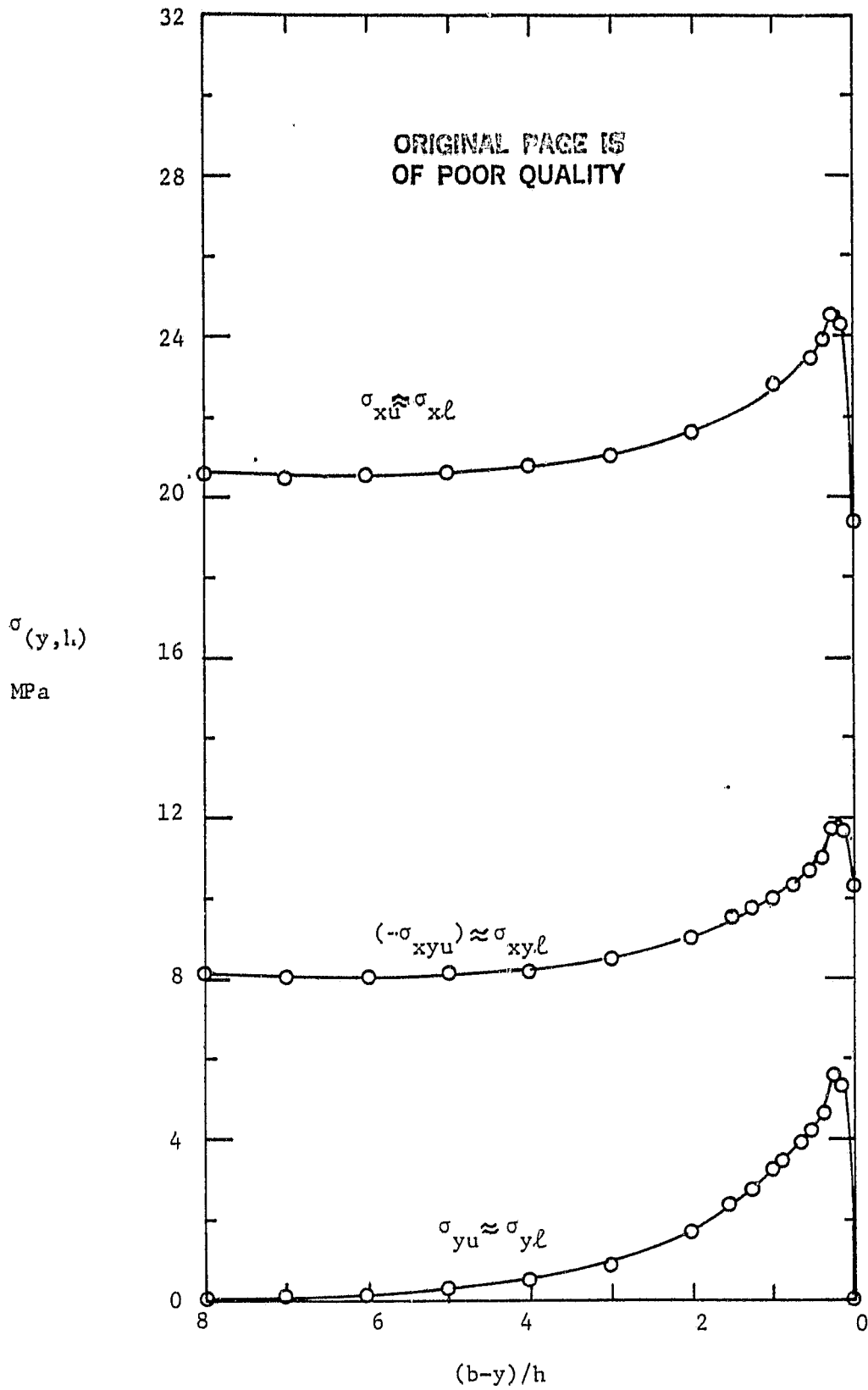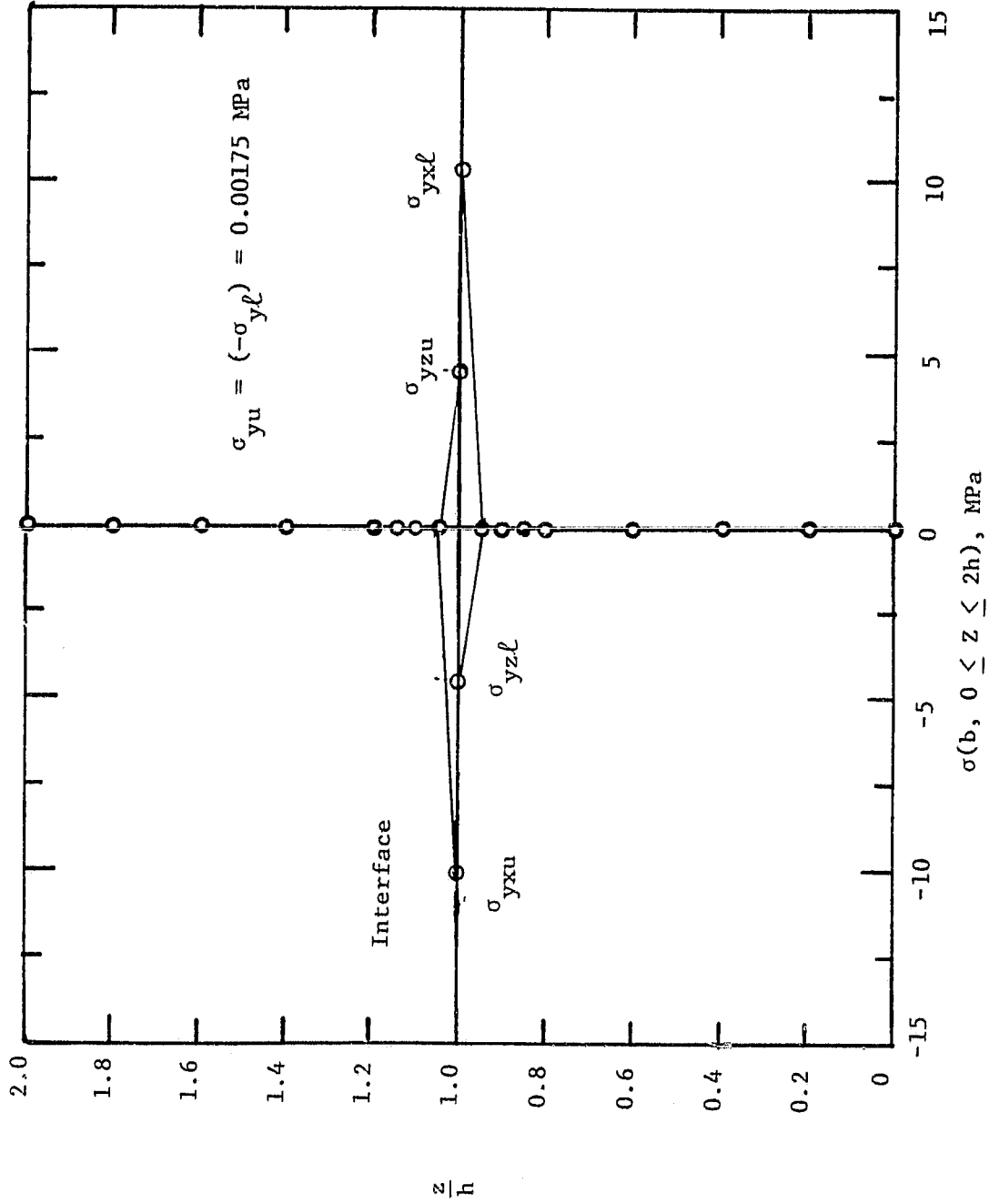
Figure 24. Stress distributions along the boundary $y = b$ for $(\sigma_y)_{ave} = (\sigma_{yx})_{ave} = (\sigma_{yz})_{ave} = 0$ at the interface corner.

-50-

APPENDIX A. FINITE-DIFFERENCE CONSIDERATIONS

Because the stress components associated with each of the three problems considered in this investigation change rapidly only in the vicinity of a stress discontinuity or a stress singularity, it is computationally effective to use a finite-difference grid with variable spacing. Finite-difference formulas for first and second order derivatives are easily derived using appropriate Taylor series. Forward, backward, and central difference formulas for first order derivatives, as well as central difference formulas for second order derivatives, are listed here for convenience. Figure A1 depicts essential parameters that appear in these equations.

The finite-difference approximations for first order derivatives are:

$$f_i' = a_1 f_i + a_2 f_{i+1} + a_3 f_{i+2} \qquad \text{(Forward)} \qquad \text{(A1)}$$

$$f_i' = b_1 f_{i-2} + b_2 f_{i-1} + b_3 f_i \qquad \text{(Backward)} \qquad \text{(A2)}$$

$$f_i' = c_1 f_{i-1} + c_2 f_i + c_3 f_{i+1} \qquad \text{(Central)} \qquad \text{(A3)}$$

where

$$\left.
\begin{array}{lll}
a_1 = -(2h+k)/h(h+k) & b_1 = \dfrac{k}{h(h+k)} & c_1 = \dfrac{-k}{h(h+k)} \\[2mm]
a_2 = \dfrac{h+k}{hk} & b_2 = \dfrac{-(h+k)}{hk} & c_2 = \dfrac{-(h-k)}{hk} \\[2mm]
a_3 = -\dfrac{h}{k(h+k)} & b_3 = \dfrac{h+2k}{k(h+k)} & c_3 = \dfrac{h}{k(h+k)}
\end{array}
\right\} \qquad \text{(A4)}$$

A prime is used to denote a first order derivative. When h and k in these formulas are replaced with ℓ and m, respectively, first order derivatives for a perpendicular direction are obtained.

The central finite-difference approximations for second order derivatives are:

$$
\begin{bmatrix} f''_{ij} \\ \ddot{f}_{ij} \\ \dot{f}'_{ij} \end{bmatrix} = \begin{bmatrix} 0 & a_1 & 0 & 0 & a_2 & 0 & 0 & a_3 & 0 \\ 0 & 0 & 0 & a_4 & a_5 & a_6 & 0 & 0 & 0 \\ a_7 & a_8 & a_9 & a_{10} & a_{11} & a_{12} & a_{13} & a_{14} & a_{15} \end{bmatrix} \begin{bmatrix} f_{i-1,\ j-1} \\ f_{i-1,\ j} \\ f_{i-1,j+1} \\ f_{i,\ j-1} \\ f_{i,\ j} \\ f_{i,\ j+1} \\ f_{i+1,\ j-1} \\ f_{i+1,\ j} \\ f_{i+1,\ j+1} \end{bmatrix} \quad (A5)
$$

where

$$a_1 = \frac{2}{h(h+k)} \qquad a_4 = \frac{2}{\ell(\ell+m)} \qquad a_7 = \frac{km}{h\ell(h+k)(\ell+m)}$$

$$a_2 = -\frac{2}{hk} \qquad a_5 = \frac{-2}{\ell m} \qquad a_8 = \frac{k(\ell-m)}{h\ell m(h+k)}$$

$$a_3 = \frac{2}{k(h+k)} \qquad a_6 = \frac{2}{m(\ell+m)} \qquad a_9 = \frac{-k\ell}{hm(h+k)(\ell+m)}$$

$$\quad (A6)$$

$$a_{10} = \frac{m(h-k)}{hk\ell(\ell+m)} \qquad a_{13} = \frac{-hm}{k\ell(h+k)(\ell+m)}$$

$$a_{11} = \frac{(h-k)(\ell-m)}{hk\ell m} \qquad a_{14} = \frac{-h(\ell-m)}{k\ell m(k+h)}$$

$$a_{12} = \frac{-(h-k)\ell}{hkm(\ell+m)} \qquad a_{15} = \frac{h\ell}{km(h+k)(\ell+m)}$$
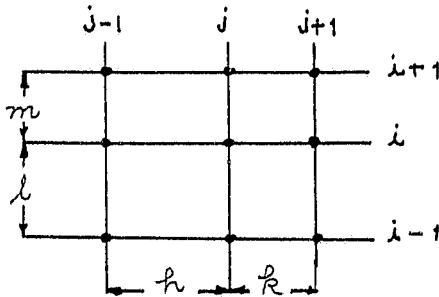
(a) Two-dimensional central differences.
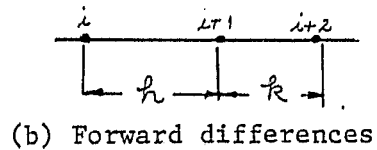
(b) Forward differences
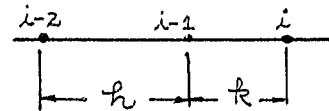
(c) Backward differences

(d) Central differences

Figure A1. Finite difference grid notations.

As an example of the derivation of these formulas consider the central difference, finite difference formulas. The Taylor series expansion of a function f(x) in the neighborhood of a point x_o is

$$f(x_o + \Delta x) = f(x_o) + f'(x_o) \Delta x + \tfrac{1}{2}f''(x_o)(\Delta x)^2 + O\{(\Delta x)^3\}. \qquad (A7)$$

Now using Figure A1-d write

$$f_{i+1} = f_i + f_i'k + \tfrac{1}{2}f_i'' k^2$$

and $\qquad f_{i-1} = f_i - f_i'h + \tfrac{1}{2}f_i''h^2 \qquad\qquad\qquad\qquad\qquad (A8)$

Simultaneous solution of these algebraic equations for f_i' and f_i'' yield the appropriate formulas given in A3 and A5. Replacing h and k by ℓ and m, respectively, gives the corresponding finite difference formulas for the perpendicular direction. Only the formula for the mixed derivative remains to be determined.

To derive a mixed second order derivative write

$$f_{i,j}' = c_{1x}f_{i-1,j} + c_{2x}f_{i,j} + c_{3x}f_{i+1,j} \qquad\qquad (A9)$$

for the line j of Figure A1-a. By differentiation

$$\dot{f}_{i,j}' = c_{1x}\dot{f}_{i-1,j} + c_{2x}\dot{f}_{i,j} + c_{3x}\dot{f}_{i+1,j}. \qquad\qquad (A10)$$

Now

$$\dot{f}_{i-1,j} = c_{1y}f_{i-1,j-1} + c_{2y}f_{i-1,j} + c_{3y}f_{i-1,j+1} \qquad\qquad (A11)$$

and similarly for $\dot{f}_{i,j}$ and $\dot{f}_{i+1,j}$. Substituting these formulas into Equation (A10) leads to a formula that expresses the mixed derivative $\dot{f}_{ij}'$ as a linear combination of the nine nodal points that surround point i,j. The literal subscripts in the coefficients c_{ix} and c_{iy} indicate these coefficients are to be evaluated using spacings in the x or y directions as the subscript dictates.

APPENDIX B

Special Material Element for Semi-Infinite Plane Problem.

The exact elasticity solution for the partially loaded, semi-infinite plane reveals that the shearing stress $\sigma_{xy}(a,o)$ tends to $\mp p/\pi$ as the points $(\pm a,o)$ are approached along the lines $x = \pm a$(see Figure 1a). However, the shearing stress, $\sigma_{yx}(\pm a,o)$, applied to the external boundary is zero. Consequently, it appears that the stress tensor is not symmetrical at these points.

The equilibrium equations on which the finite difference solution is based incorporate symmetry of the stress tensor at all interior points. Moreover, no special expressions exist that define the relationship between shearing stress components at points where the stress tensor is not symmetrical. Therefore, the classical finite difference procedure can not be expected to detect such an anomaly.

Part of this investigation involves examining the effectiveness of introducing a moment equation for a finite element of material near point (a,o). The purpose of the moment equation is to establish a relationship among the shearing stresses of an unsymmetrical stress tensor.

Supposedly, the moment equation associated with a finite element of material near the boundary point (a,o) replaces a finite difference boundary condition involving the shearing stress $\sigma_{yx}(a,o)$. Problems arise, however, because once the finite element of material has been introduced it is inappropriate to ignore force equilibrium of the element. Thus, three equilibrium equations are obtained to replace two finite difference boundary conditions at point (a,o). Since no new independent variables have been introduced, the resulting system of equations is over specified.

Even if it were possible to introduce an additional, appropriate, independent stress variable at point (a,o) the system of equations, when expressed in terms of displacements, would remain over specified unless unsymmetrical stress-strain relations are introduced. This latter concept represents a considerable complication and is ignored in the analyses made in this investigation.

Not withstanding the analytical difficulties enumerated in the preceding paragraphs, two separate finite elements of material near point (a,o) were considered. These elements are shown in Figures B1 and B2.

The element shown in Figure B1 is based on first order Lagrange interpolations of the stresses along its edges. Moment equilibrium for the material element yields the equation

$$\int_o^m (m-y)\sigma_x(a,y)\,dy - \int_o^m \ell\sigma_{xy}(a,y)\,dy$$

$$+ \int_o^m (m-y)\sigma_x(a-\ell,\ y)\,dy - \int_{a-\ell}^a (x-a+\ell)\sigma_y(x,m)\ dx = 0. \quad (B1)$$

Using the first order Lagrange interpolations for stresses along the edge of the element leads to the algebraic equation

$$\frac{m^2}{6}(2\sigma_{x4} - 2\sigma_{x2} + \sigma_{x3} - \sigma_{x1}) - \frac{mh}{2}(\sigma_{xy4} + \sigma_{xy3})$$

$$+ \frac{h^2}{6}(\sigma_{y1} + 2\sigma_{y3}) + \frac{ph^2}{2} = 0. \quad (B2)$$

Here σ_{xi}, σ_{yi}, σ_{xyi} are components of stress at the finite difference nodes that coincide with the corners of the element.

Equation B2 is expressed in terms of displacements (u,v) by means

of the symmetrical stress-strain relations (This is not a strictly

legitimate procedure since, if the stress tensor is assumed to be

unsymmetrical, the strain tensor must also be unsymmetrical). Equation B2

expressed in terms of displacements is not recorded here because nothing

of significant interest can be extracted from it.

Using only the moment equation for the material element and a finite

difference normal stress boundary condition, encouraging, but not exact,

agreement with the exact solution was observed for all three stress

components $(\sigma_x, \sigma_y, \sigma_{xy})$,

Because two of the three equilibrium equations associated with the

material element were ignored it is quite possible that whatever agreement

that exists, is, probably, gratuitous.

The second material element is shown in Figure B2 and is based on

second order Lagrange interpolations of stresses along its edges, Thus,

approximations of stresses along the edges of the element are of the

same order of approximation as the finite difference formulas used to solve

the equilibrium equations. It was felt that this material element

represented a better meshing with the finite difference approximations of

the equilibrium equations than the first element and should, therefore,

lead to even better agreement with the exact solution, In some respects,

this was not to be the case.

Moment equilibrium and force equilibrium for the y direction yield the

formulas

$$\int_0^m y[\sigma_x(\tfrac{h}{2}, y)\ dy] - \int_0^m h[\sigma_{xy}(\tfrac{h}{2}, y)\ dy] + \int_{-\frac{h}{2}}^{\frac{h}{2}} (x + \tfrac{h}{2})[\sigma_y(x,o)dx]$$

$$-\int_0^m y[\sigma_x(-\tfrac{h}{2},y)dy] + \frac{ph^2}{8} = o, \qquad (B3)$$

And

$$-\int_{-\frac{h}{2}}^{\frac{h}{2}} \sigma_y(x,o)\,dx - \int_0^m \sigma_{xy}(-\frac{h}{2},\ y)\,dy + \int_0^m \sigma_{xy}(\frac{h}{2},\ y)\ dy - \frac{ph}{2} = 0. \qquad (B4)$$

Using second order Lagrange interpolations for stresses along the edges of the material element leads to two formulas that involve the stress components (σ_x, σ_y, σ_{xy}) at the nine finite difference nodes that are nearest to the element. Subsequent use of the symmetrical stress-displacement relations leads to two equations in the displacements (u,v). These equations are not presented here because of their length, and because no new insights can be derived from them.

Using only the moment equilibrium equation and the finite difference normal stress boundary condition (Similar to the procedure used in the analysis of the first material element) it was observed that the stress components σ_x and σ_y agreed well with the exact solution, but σ_{xy} was grossly over estimated.

Introducing the force equilibrium equation for the y direction, together with the moment equilibrium equation, revealed that σ_x, σ_y, and σ_{xy} were each in substantial disagreement with the exact solution for these stress components near the boundary point (a,o).

The results of the numerical studies presented in this appendix indicate that substantial analytical difficulties are encountered when a finite material element is introduced near the point (a,o) to account for a lack of symmetry in the stress tensor.

To be analytically rigorous unsymmetrical stress-strain relations should be used, and all three equilibrium equations associated with the element should be used.

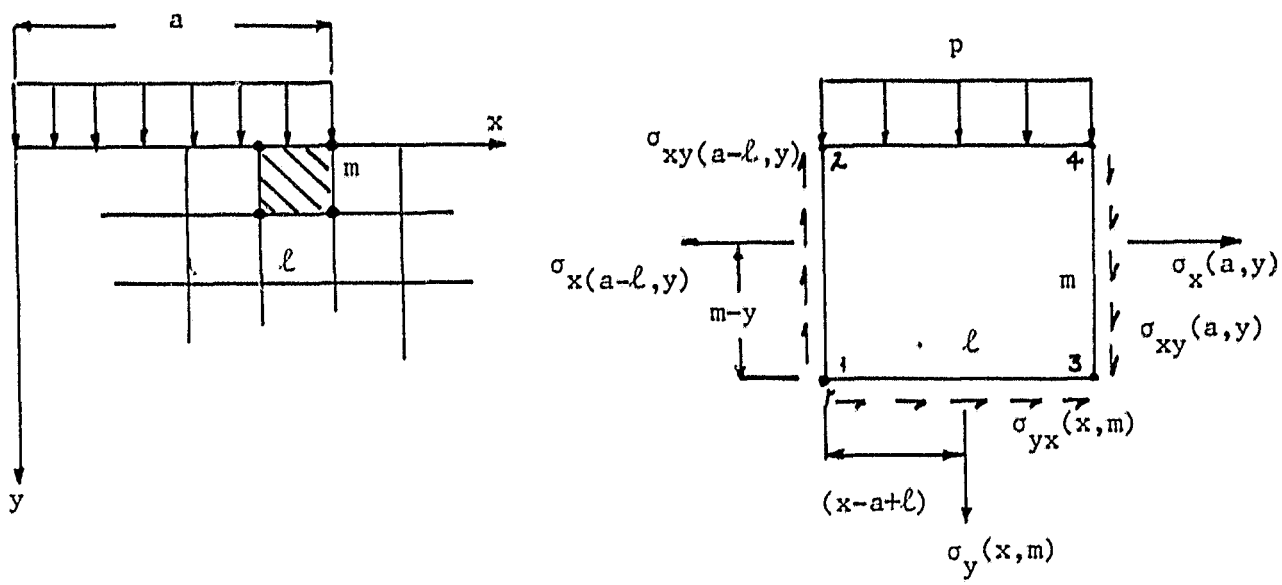FIGURE B1. Finite material element using linear variation of stresses along its edges.
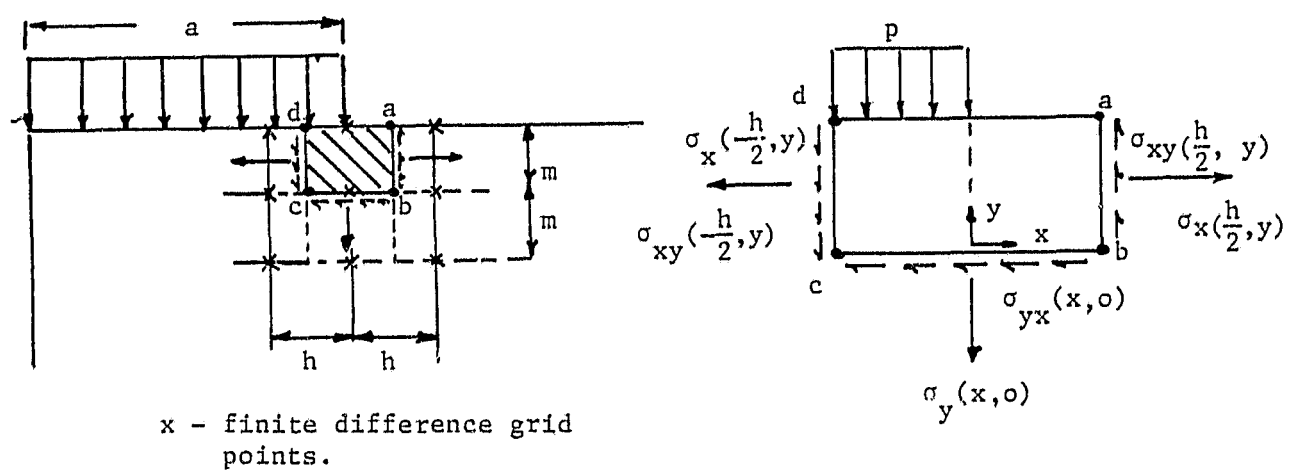

x - finite difference grid points.

FIGURE B2. Finite material element using quadratic variation of stresses along its edges.

USER INSTRUCTIONS FOR SEMI-INFINITE PLANE UNDER PARTIAL LOAD.

This appendix contains information describing the cards that must be prepared by the program user and the output information to be expected.

INPUT INFORMATION

FIRST CARD (3F10.0, 4I5)

columns	1-10	Poisson's ratio, ν
	11-20	Modules of elasticity, E(psi)
	21-30	Uniform pressure, p (lb/in)
	31-35	Column number of the grid line through point A, (NDSCN). NDSCN = 3 in Figure C2.
	36-40	NROW, number of grid lines parallel to the x-axis. NROW = 7 in Figure C2.
	41-45	NCOL, number of grid lines parallel to the y-axis. NCOL = 9 in Figure C2.
	46-50	NPAR, parameter used to select boundary conditions imposed at point A. See Boundary Conditions.

SECOND CARD (6F 10.0)

Grid line spacings (inches) in the x-direction, dx_i are shown in Figure C2.

THIRD CARD (6F 10.0)

Grid line spacings (inches) in the y-direction, dy_i are shown in Figure C2.

OUTPUT INFORMATION

Input data is printed, followed by the stress components σ_x(SIGX), σ_y(SIGY), and σ_{xy}(SIGXY) associated with the line x = a. Stresses along the loaded boundary are also printed.

MINIMUM DIMENSIONS FOR ARRAYS

If program capacity needs to be enlarged the following arrays require minimum dimensions as indicated.

DIMENSION   DX(NCOL-1), DY(NROW-1), ST(2, 18), XST (MA),
            SIGX(NROW), SIGY(NROW), SIGXY(NROW), R(NEQ),
            ID(2, NUMNP), IDIAG(2), ID1(18), IDD(NROW),
            Y(NROW)

NCOL — Number of grid lines parallel to the y-axis.

NROW — Number of grid lines parallel to the x-axis.

NUMNP — Number of nodal points (NROW*NCOL).

. NEQ — 2*NUMNP - NROW - NCOL + 1

MA — NEQ*(8*NROW-3)-(2*NROW-1)*(4*NROW-1)

BOUNDARY CONDITIONS SPECIFIED AT FINITE DIFFERENCE GRID POINTS
(See Figure C2).

●   Equilibrium equations

⊗   u=v=0 (x and y displacements)

○   u=0, $\sigma_{xy} = 0$

x $\sigma_{xy}=0$, $\sigma_y = -p$

■   (1) NPAR=1 — $\sigma_y = -p/2$, $\sigma_{xy} = 0$

        (2) NPAR=2 — $\sigma_y = -p$, finite moment equation.

        (3) NPAR=3 — $\sigma_y = -p/2$, finite moment equation.

        (4) NPAR=4 — Finite force and finite moment equations.

        (5) NPAR=5 — $\sigma_y = -p$, $\sigma_{xy}=0$.

        (6) NPAR=6 — $\sigma_y = -p/2$, modified moment equation.

        (7) NPAR=7 — Modified finite force and finite moment
                        equations.

△ $\sigma_y = \sigma_{xy}=0$

□ $\sigma_x = \sigma_{xy}=0$

▲ v=0, $\sigma_{xy}=0$

NOTES:

(1) H and V in Figure C2 should be large enough to validate the assumption that the stresses on the bottom boundary and right boundary are negligibly small.

(2) A vertical grid line through point A is required.

(3) The number of grid lines to the left of point A must be greater than two.

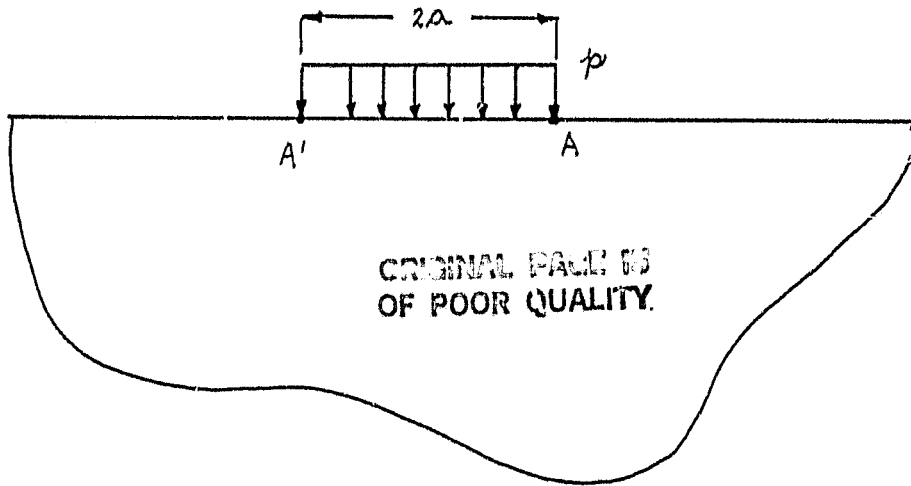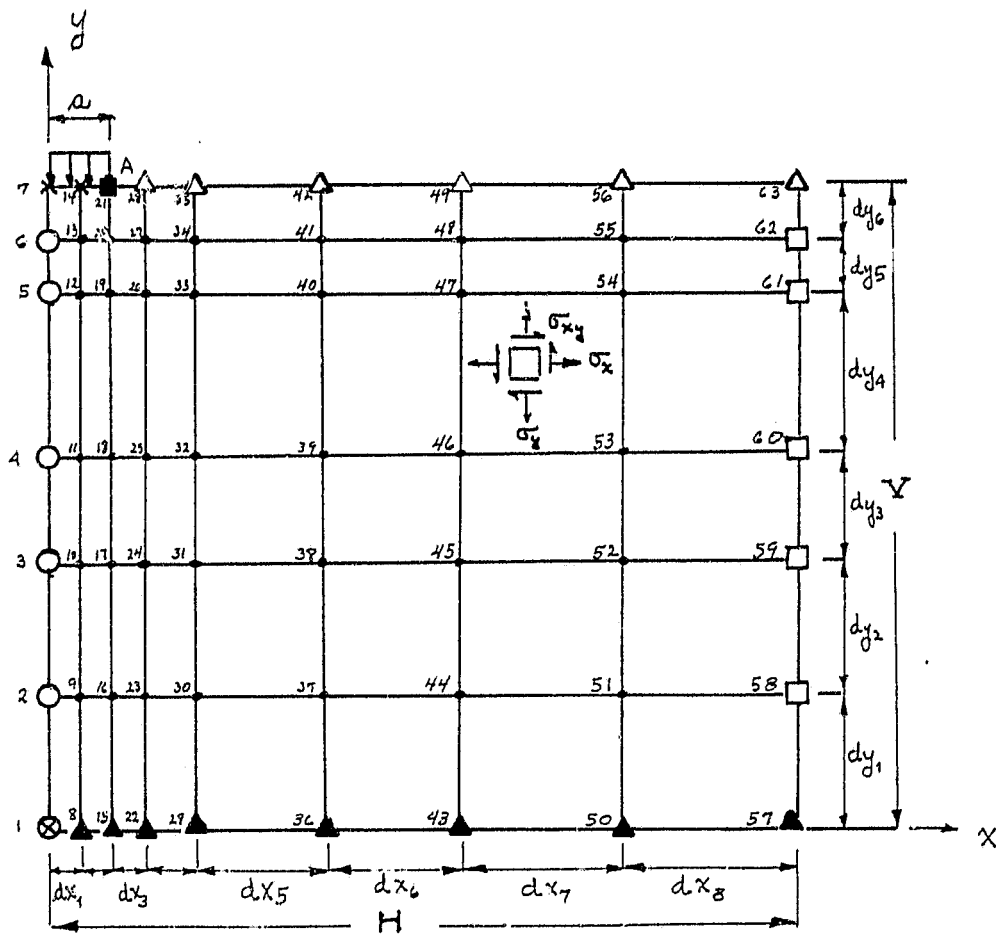(4) Numbering scheme for nodal points is shown in Figure C2.

FIGURE C1.

FIGURE C2.

APPENDIX D

USER INSTRUCTIONS FOR BIMETALLIC PLATE IN TENSION

This appendix contains information describing the cards that must be prepared by the program user and the output to be expected.

INPUT INFORMATION

FIRST CARD (3F10.0, 2I5)

Columns	1-10	Poisson's ratio, ν
	11-20	Modulus of elasticity, E(psi)
	21-30	Uniform pressure, p (lb/in)
	31-35	NROW - Number of grid lines parallel to the x axis.
	36-40	NCOL - Number of grid lines parallel to the y axis

SECOND CARD (6F10.0)   Finite difference spacings for the x direction (dx_i) (inches).

THIRD CARD (6F10.0)   Finite difference spacings for the y direction (dy_i) (inches).

OUTPUT INFORMATION

Input data are printed followed by the stress components σ_y(SIGY) and σ_{xy}(SIGXY) along the bond line.   Stress components σ_x(SIGX) and σ_{xy}(SIGXY) are printed for the stress free edge. The net normal force and net shear force acting on the bond line are also printed.

MINIMUM DIMENSIONS FOR ARRAYS

If program capacity needs to be enlarged the following arrays require minimum dimensions as indicated.

DIMENSION   DX(NCOL-1), DY(NROW-1), ST(2,18), XST(MA), X(NCOL), Y(NROW), R(NEQ), ID(2, NUMNP), IDIAG(2), ID1(18), SIGXYL(NROW), SIGXL(NROW), SIGXYT(NCOL), SIGYT(NCOL).

NCOL - Number of grid lines parallel to the y axis.

NROW - Number of grid lines parallel to the x axis.

NUMNP - Number of nodal points (NCOL*NROW).

NEQ - Number of equations = 2*(NUMNP-NROW)-NCOL + 1

MA - (8*NROW-3)*NEQ-(2*NROW-1)*(4*NROW-1)

BOUNDARY CONDITIONS SPECIFIED AT FINITE DIFFERENCE GRID POINTS
(See Figure D2)

⊕   Equilibrium equations.

x   u=v=0 (x and y displacements)

□ $\sigma_{xy} = \sigma_y = 0$

Δ $\sigma_{xy} = 0$ $\sigma_x = p$

0      $v=0,\ \sigma_x = p/2$

● $v=0,\ \sigma_{xy} = 0$

Notes:

(1) Subroutine DCSPQU is a subroutine from PORT Mathematical
Subroutine Library and is not provided with the main program.
This subroutine is used to integrate the stresses along a
boundary to determine the net normal force and net shear
force on that boundary. If users do not have access to
PORT subroutines, delete program statements delimited by
comment statement C/////// in the main program.

(2) Subroutine DGELB is a subroutine from the IBM Scientific
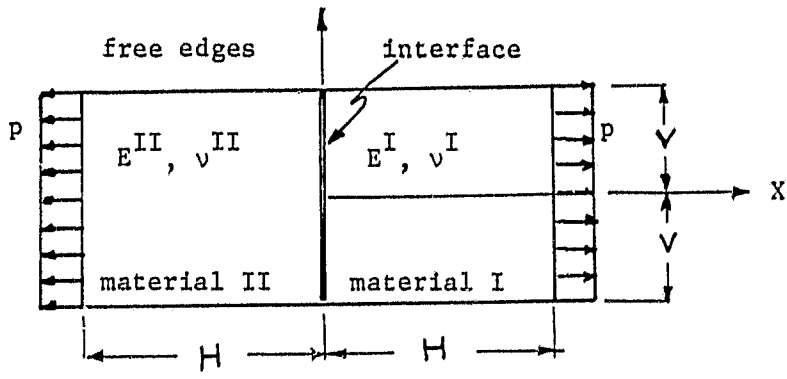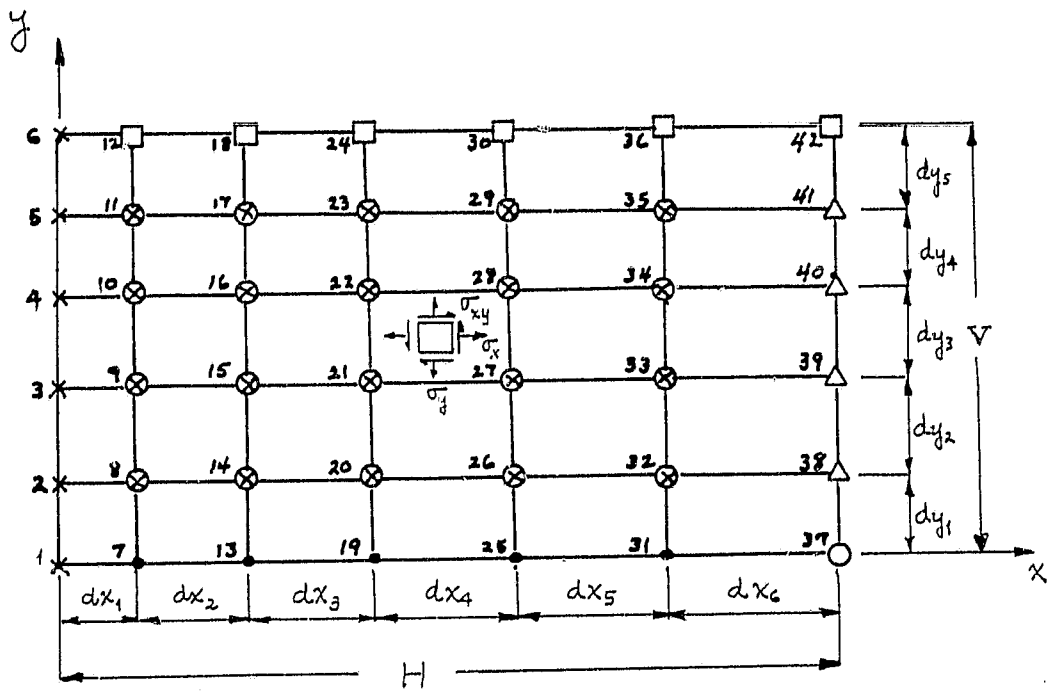Subroutine Package and is included with the main program.

FIGURE D1.

FIGURE D2.

APPENDIX E

USERS INSTRUCTIONS FOR UNIFORM STRAIN OF LAYERED COMPOSITE

This appendix contains information describing the cards that must be prepared by the program user and the output information to be expected.

INPUT INFORMATION

FIRST CARD (3F 20.0)

columns	1-20	Poisson's ratio, ($\nu_{12} = \nu_{23} = \nu_{13}$)
	21-40	Shear modulus ($G_{12} = G_{13} = G_{23}$, Pascal)
	41-60	Modulus of elasticity parallel to fiber direction, (E_{11}, Pascal)

SECOND CARD (2F20.0, 3I10)

columns	1-20	Moduli of elasticity perpendicular to the fiber direction ($E_{22} = E_{33}$, Pascal).
	21-40	Applied uniform strain ε_o
	41-50	NROW – Number of grid lines parallel to the y axis.
	51-60	NCOL – Number of grid lines parallel to the z axis.
	61-70	INT – Row number for the grid line coincident with the interface between the +45 and -45 plies. (INT=5 in Figure E2).

THIRD CARD (6F10.0)

Grid line spacings (meters) in the y direction, dy_i are shown in Figure E2.

FOURTH CARD 96F10.0)

Grid line spacings (meters) in the z direction, dz_i are shown in Figure E2.

OUTPUT INFORMATION

Input data are printed, followed by the stress components σ_z(SIGZ), σ_{zx}(SIGZX), σ_{zy}(SIGZY), σ_x(SIGX), σ_y(SIGY), and σ_{xy}(SIGXY) along the interface. Subsequently the stress components σ_y, σ_{yx}, and σ_{yz} along the stress free edge are printed.

Subscripts u or ℓ are affixed to a stress component to indicate its relation to either the +45 or the -45 ply, respectively.

MINIMUM DIMENSIONS FOR ARRAYS

If program capacity needs to be enlarged the following arrays require minimum dimensions as indicated.

DIMENSION ST(3,27), ID1(27), ID1AG(3),
DY(NCOL-1), DZ(NROW-1), Z(NROW),
SGY(NROW), SGXY(NROW), SIGX(NROW), XST(MA),
ID(3, NUMNP), R(NEQ), Y(NCOL)

NCOL — Number of grid lines parallel to the z axis.

NROW — Number of grid lines parallel to the y axis.

NUMNP— Number of nodal points (NCOL*NROW)

NEQ — Number of equations (3*NUMNP-2*NROW - NCOL + 3)

MA — NEQ*(12*NROW+1)-(3*NROW)*(6*NROW + 1)

BOUNDARY CONDITIONS SPECIFIED AT FINITE DIFFERENCE GRID POINTS
(See Figure E2). Six different programs EDGSTRS1, EDGSTR2,..., EDGSTRS6 incorporate the following boundary conditions.

■ $U=V=W=o$ (x, y, and z displacements)

⊡ $U=V=W_{,y}=0$

△ $\sigma_z=\sigma_{zx}=\sigma_{zy}=0$

▢ $\sigma_y=\sigma_{yx}=\sigma_{yz}=0$

◮ $W=U_{,z}=V_{,z}=0$

✕   Equilibrium equations for the +45 ply.

●   Equilibrium equations for the −45 ply.

○   Stress continuity along the interface ($\sigma_{zu}=\sigma_{z\ell}$; $\sigma_{zxu}=\sigma_{zx\ell}$, and $\sigma_{zyu}=\sigma_{zy\ell}$)

▲ $\begin{cases} U=V=W_{,y}=0 \text{ for EDGSTRS1 through EDGSTR5} \\ \text{Stress continuity between plies for EDGSTRS6} \end{cases}$

⊗ $\begin{cases} W=U_{,z}=V_{,z}=0 \text{ for EDGSTRS1} \\ \sigma_y=\sigma_{yx}=\sigma_{yz}=0 \text{ for EDGSTRS2 through EDGSTR6} \end{cases}$

⊠ $\begin{cases} \text{Interlaminar stress continuity for EDGSTRS1, EDGSTRS2, and EDGSTRS6} \\ \sigma_{yu}=\sigma_{yxu}=\sigma_{yzu}=0 \quad \text{for EDGSTRS3} \\ \sigma_{y\ell}=\sigma_{yx\ell}=\sigma_{yz\ell}=0 \quad \text{for EDGSTRS4} \\ \sigma_{yu}+\sigma_{y\ell}=\sigma_{yxu}+\sigma_{yx\ell}=\sigma_{yzu}+\sigma_{yz\ell}=0 \text{ for EDGSTRS5} \end{cases}$

NOTES:

(1) These programs determine the distributions of the stress components along the interface between the +45 and -45 plys of a $\left[\pm\ 45\right]_s$ laminate under uniform axial strain with laminate properties $E_{11} \neq E_{22}$, $E_{22}=E_{33}$, $G_{12} = G_{13} = G_{23}$, and $\nu_{12} =\nu_{23} =\nu_{13}$

(2) Subroutine DGELB is a subroutine from the IBM Scientific Subroutine Package and is provided with the main program.

(3) Subroutine DCSPQU is a subroutine from PORT Mathematical Subroutine Library and is not provided with the main program. This subroutine is used to integrate the stresses along a boundary to determine the net normal force and net shear forces on that boundary. If users do not have access to PORT subroutines, delete program statements delimited by comment statement C///// in the main program.
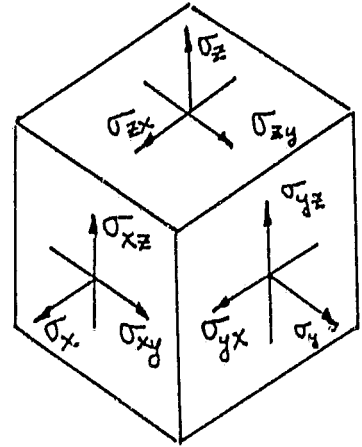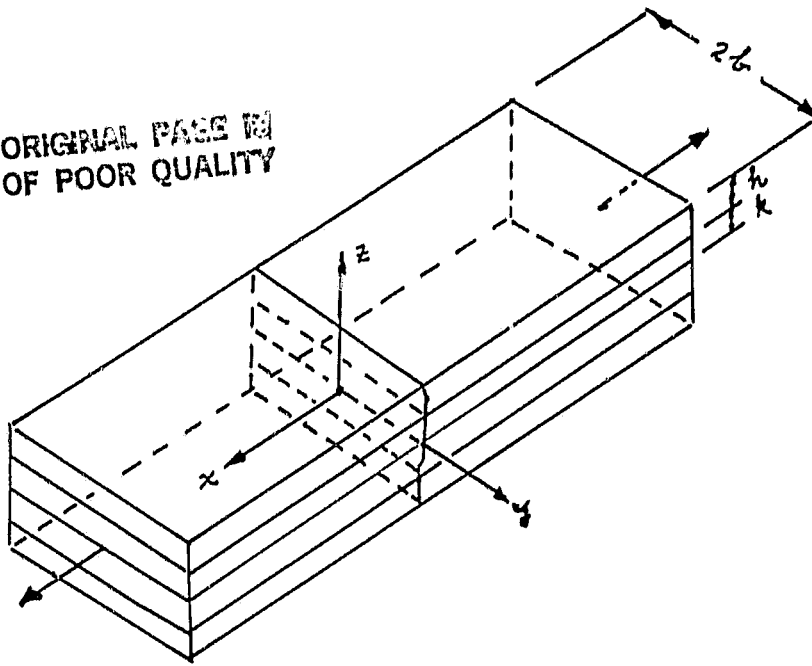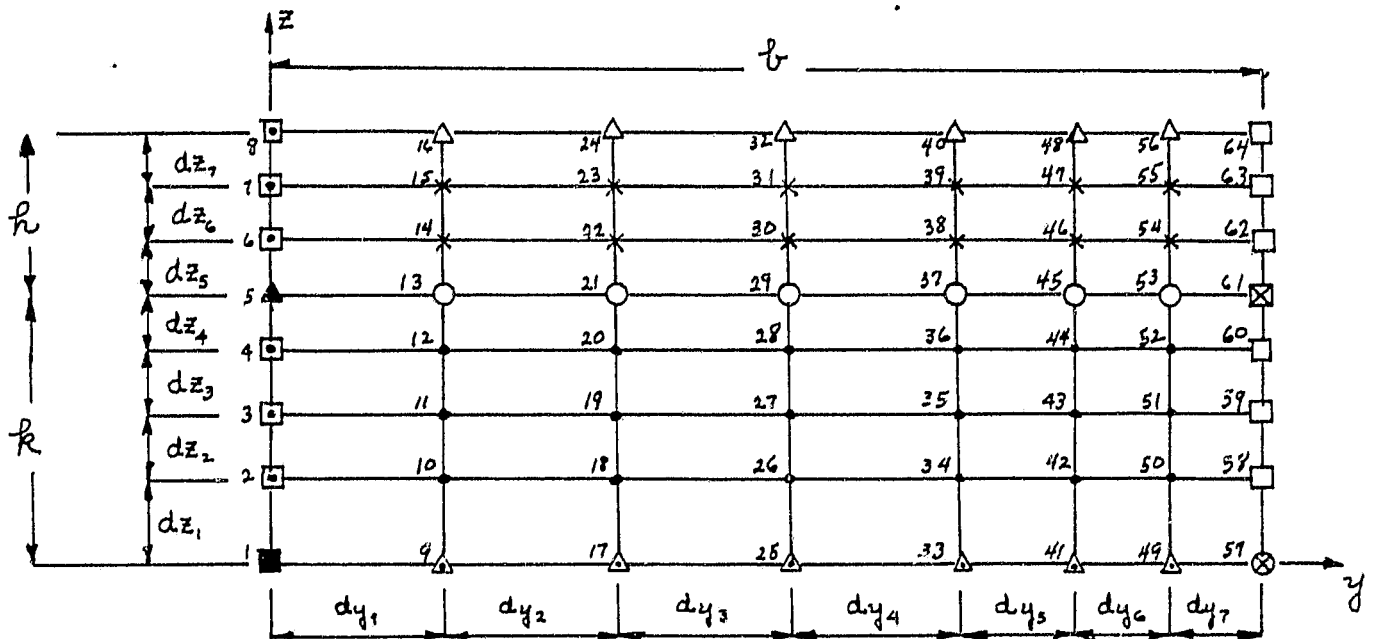
FIGURE E1.

FIGURE E2.